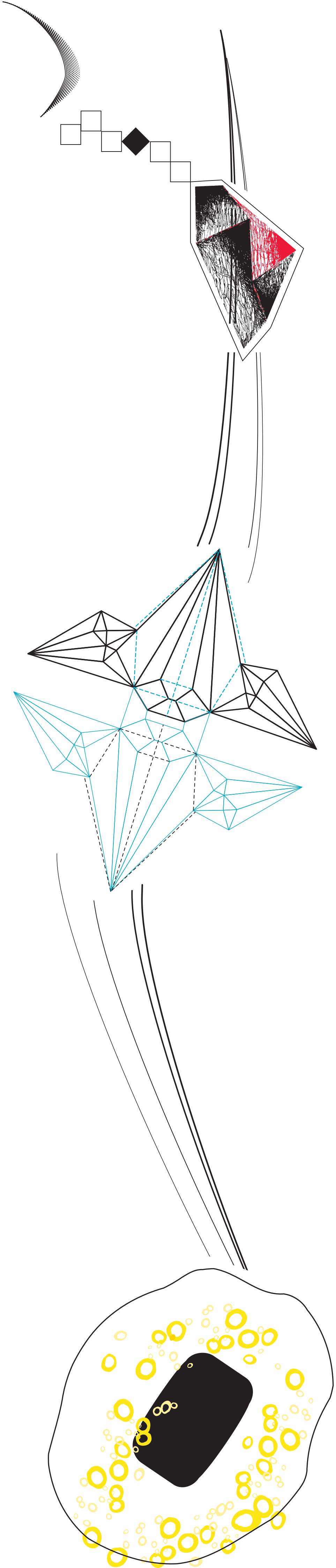

Chemical & Process Engineering

Two (L-L) and Three (G-L-L) Phase Extraction Processes in Capillaries with Heterogeneous Surface Wettability.

N.A.B. Timmerhuis, BSc.
October 2017

Faculty of Science and Technology
Research group: Soft matter, Fluidics and Interfaces

Committee:
Prof.Dr.Ir. R.G.H. Lammertink (chairman)
Dr.Ir. B. Schuur (external member)
Dr. J.A. Wood (supervisor)
H. Bazyar, MSc. (daily supervisor)

UNIVERSITY OF TWENTE.

Abstract

The effect of heterogeneous surface wettability was studied for two and three phase extraction. The model system consisted of 1 wt% acetic acid (solute) in water (carrier) with 1-octanol as solvent, nitrogen gas was added for the three phase extraction. A round capillary of 1.05 mm inner diameter and 150 mm length was used to study the influence. Two and three phase extraction performance was determined in a homogeneous hydrophilic capillary and two capillaries with heterogeneous wettability (alternating hydrophilic and hydrophobic patcher) with patterning lengths of 1.0 and 6.0 mm. Phase inversion, adhesion and passing was shown for the two phase system in the 6.0 mm patterning while only adhesion and passing was shown for the 1.0 mm patterning. The three phase extraction showed passing with organic phase as continuous phase instead of water, which is the expected pattern for a hydrophobic capillary. The extraction performance was enhanced primarily by the two phase extraction in heterogeneous capillary, where the organic to water ratio can be decreased from 2 to 1 with 6.0 mm patterning. For the three phase extraction the organic to water ratio could only be lowered to 1.33 (compared to 2) with the 6.0 mm patterning.

Acknowledgements

This master project would not be possible without the help of many people. I would like to express my gratitude towards everyone who helped me during project with the project itself or with creating a distraction every now and then. Some people I would like to thank personally. Firstly, my thanks to Rob Lammertink for letting me be a part of the Soft matter, Fluidics and Interfaces group for my master assignment. A special thanks to Hani Bazyar, my daily supervisor, for her commitment towards my project. Hani always helped me with a lot of positive energy, when something did not work on the lab, again. Next, I would like to thank Jeff Wood for his insights during meetings and the COMSOL modelling. Both Jeff and Hani always inspired me to go the extra mile. Thanks to Boelo Schuur for being part of my committee. I would also like to thank everybody from the SFI group and especially Jan van Nieuwkasteele, for his countless hours cleaning and hydrophobizing capillaries in the cleanroom and his help with building and improving the setup. Last, but not least, I want to thank my family and friends for their support during my studies and this project.

Contents

Nomenclature

Greek symbols

α	Slug length over the total unit cell length	
β	Fitting parameter	
ϵ	Phase holdup	
γ	Interfacial tension	N/m^2
μ	Viscosity	Pa.s
ϕ	Tangent angle	°
ρ	Density	kg/m^3
σ	Surface tension	N/m
τ	Residence time	s
θ	Contact angle	°

Roman symbols

A	Hamaker constant	J
a	Interfacial area	m^2/m^3
D	Slug length	m
d	Channel diameter	m
E	Extraction efficiency	%
g	Gravity force	m/s^2
h	Capillary rise	m
h	Film thickness	m
K	Partition coefficient	
k	Fitting parameter	
k_L	Mass transfer coefficient	m/s
$k_L a$	Volumetric mass transfer coefficient	1/s
L	Channel length	m
L_d	Slug length	m

n	Refractive index	
P	Pressure	Pa
Q	Flow rate	µL/min
R	Organic to water ratio	
r	Channel radius	m
R_{aq}	Rate constant	m/s
s	Arc length	m
s	Error	
u	Superficial velocity	m/s
w	Weight fraction	
w	Width of the channel	m
w^*	Weight fraction at equilibrium	

Subscripts

a	Apparent
aq	Aqueous phase
c	Continuous phase
d	Dispersed phase
i	Real
o	Outer
org	Organic phase

Superscripts

α	Inside
β	Outside
ow	organic-water
so	solid-organic
sw	solid-water

Chapter 1

Introduction

Extraction is a common separation technique which is used as alternative for distillation [1]. Liquid-liquid extraction is preferred over distillation when there are small amounts of analytes in the feed, for the recovery of heat sensitive materials, separation of azeotropic mixtures, or if high-boiling components are present in relatively small amounts in an aqueous solution. The main disadvantage of liquid-liquid extraction lies in the low mass transfer rate, which makes the column efficiency low. Additionally, two (or more) distillation columns are needed in order to separate the solvent, feed and product from each other.

One of the key features of liquid-liquid extraction is the solvent [1]. Usually, an organic solvent is used to extract from an aqueous feed and vice versa. The ideal solvent has a high selectivity towards the solute and minimal solubility in the carrier. The volatility difference between solvent and solute should be sufficient in order to get an easy separation in the distillation columns. Besides the solvent, there are other important variables whilst designing an extraction column. Every type of equipment has its own advantages and disadvantages, depending on all the operational factors like feed flow rate, composition, temperature, pressure, stage configuration etc.

Micro scale liquid-liquid extraction has gained interest over the past years, especially in the field of pharmaceutics and analytical chemistry [2; 3]. Micro scale extraction has a shorter transfer length and increased interfacial area, which improves mass transfer.

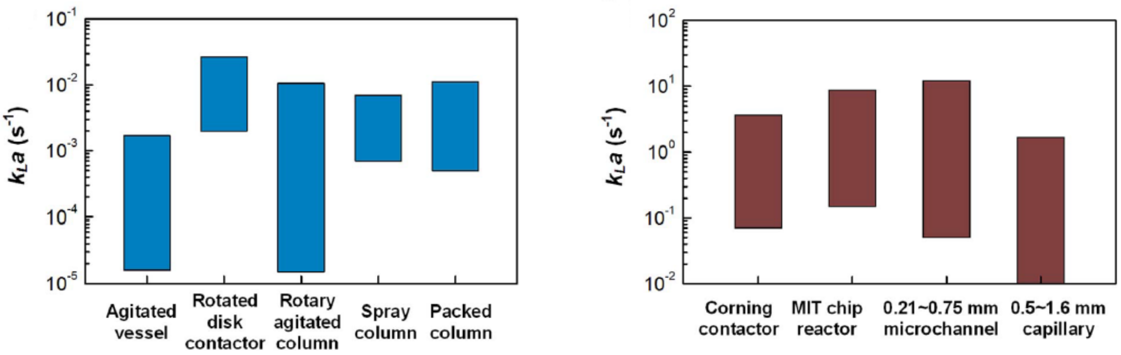

(a)

(b)

Figure 1.1: Differences in volumetric mass transfer coefficient. (a): Macro systems. (b): Micro systems. Adapted from [4].

Figure 1.1 shows the different order of magnitude in volumetric mass transfer coefficient for macro (a) and micro systems (b) [4]. The volumetric mass transfer coefficient ($k_L a$) increases two to three orders of magnitude in micro systems compared to macro systems. The bottlenecks of micro scale extraction lies in the separation methods and scaling up the process. Also, the flow is laminar which limits transfer efficiency due to a lack of vortices and mixing [5]. The micro scale extraction can be enhanced to overcome some mass transfer limitations and possibly make it more attractive for up scaling.

1.1 Enhanced micro scale liquid-liquid extraction

The enhancement can roughly be divided in four categories: geometry, packing, three-phase flow (gas-liquid-liquid) and wettability, shown in Figure 1.2. The main features of each process intensification will be shortly discussed.

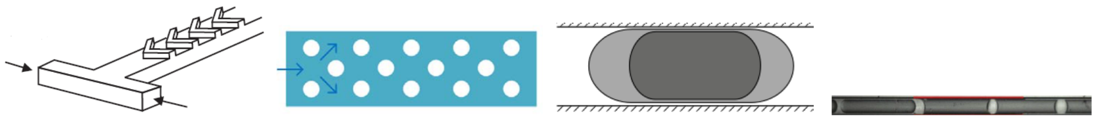

(a) (b) (c) (d)

Figure 1.2: Different enhancement methods for micro scale liquid-liquid extraction are illustrated. (a): Geometry with an Herringbone pattern, adapted from [6]. (b): Packed bed, adapted from [4]. (c): Gas addition [7]. (d): Wettability, adapted from [8].

Geometry The change in geometry of the channel causes rupture or coalescence of emulsions, which are small droplets of one immiscible liquid in another [5; 9], which is usually used in micromixers. Micromixers can be divided in two categories: passive and active [6]. Passive micromixers do not need external energy, which makes them more robust, stable in operation and easily integrated in complex systems. Active micromixers create a disturbance which is generated by an external field. An external power source is needed which makes the fabrication more complex. Many different geometries can be used for passive micromixers, for example a herringbone pattern shown in Figure 1.2(a). The mixing efficiency is highly dependent on the flow characteristics like the Reynolds number. The geometries used in micromixers can also be used for liquid-liquid extraction, creating more disturbance in the flow which increases the mass transfer. However, the main disadvantage is a large pressure drop in the mixer, which needs to be overcome by additional energy.

Packed bed Packed bed is a common method for macro scale liquid-liquid extraction [1]. The decrease in axial dispersion is one of the main advantages of a packed bed. The interfacial area is increased whilst the packing breaks large drops into smaller droplets. Su et al. [10] reported an increase in extraction efficiency from 46-61% to 81-96% by including quartz sand micro-particles as packing in a stainless steel microchannel. The droplet size decreased up till 10 µm for a water-succinic acid-n-butanol system, increasing the specific area approximately 100 times. Just as for geometry, the large pressure drop is the main disadvantage of this technique.

Gas addition The addition of a gas in an extraction process can be done on micro and macro scale. Gas is added on the macro scale to prevent backmixing problems in non-agitated columns

[11]. The inert gas is added to function as a mixing agent by creating a more turbulent flow, increasing the mass transfer area. Wang et al. (2015) was able to increase the extraction efficiency with 16-23 times by the addition of gas in a liquid-liquid extraction on micro scale [5]. It was achieved by adding gas inside the solvent, making a double emulsion and decreasing the mass transfer distance between water and solvent. This resulted in an increase of the extraction efficiency. Assmann et al. (2012) enhanced the mass transfer coefficient by adding the inert gas in a parallel flow regime, creating slug flow with internal circulations in the liquid slugs [3]. Tan (2011) focussed on the dispersion mode for a three-phase system, increasing the extraction efficiency 10-30 times [12]. Mandalahalli (2015) stated that the increasing extraction efficiency is due to the increase in interfacial area [7]. However, the film layer between the gas and wall gets easily saturated and does not get refreshed due to the internal circulation which are not strong enough to mix the oil and water phase. In conclusion it can be said that the addition of the gas improves the extraction efficiency by increasing the interfacial area but a new mass transfer limitation is formed by the saturated oil film layer between the gas and water phase.

Wettability Modifying the wettability in a microchannel has been used for increasing the stability of parallel liquid-liquid flows [13], creating a stable interface for chemical reactions [14]. O'Loughlin et al. (2013) approached modified wettability as an alternative approach to mechanical pumping and valving with promising results for capillary-driven flow [15]. Zhao et al. (2008) studied the influence of surface wettability [16]. The modification of wettability gave more stable flows at low Reynolds number. At higher Reynolds number, the flow was not influenced by surface modification. The mass transfer coefficient in the microchannels was one or three orders of magnitude higher compared to large scale contactors. Meng et al. (2015) successfully patterned a microfluidic capillary, alternating the hydrophilic and hydrophobic wall inside the capillary [8]. The alternating wettability caused the slug flow to adhere on the surface, create phase inversion or the slugs were broken, resulting in a chaotic turbulent flow. In conclusion it can be said that by changing the surface wettability the flow can be stabilized or broken down, dependent on the surface properties and periodicity.

1.2 Problem Statement

The research of Mandalahalli [7] indicates that the small film layer in the oil phase around the gas slug is saturated very fast for gas-liquid-liquid flows. The refreshing of the film layer does not occur, creating a mass transfer limitation. This limitation could be overcome by introducing heterogeneous surface wettability. By changing and patterning the wettability of the capillary, the saturated film layer can mix with the bulky slug, which decreases the mass transfer limitation. The focus of this research lies on controlling the degree of mixing, created by the heterogeneous surface wettability of the capillary, in order to control the extraction efficiency. Different patterning lengths and flow rates, thus slug properties, are used to study their influence on the extraction efficiency.

Chapter 2

Background and Motivations

A literature study is performed for more in-depth insights in the project. As model system, 1 wt% acetic acid in water with 1-octanol is chosen. Diluted acetic acid is a common byproduct in the biodiesel production. The literature background is first focussed on the extraction system and its chemistry. Secondly, the relation between the acting forces and flow patterns is explained in hydrodynamics. The effect of heterogeneous wettability is discussed as third. The mass transfer performance is also quantified before setting the research goals.

2.1 Chemistry

Acetic acid is dissociated in water, as shown in Eq. (2.1) [1]. The process is limited by the equilibrium.

$$\mathrm{CH_3COOH + H_2O \rightleftarrows CH_3COO^- + H_3O^+}, \qquad K_\mathrm{a} = \frac{[\mathrm{CH_3COO^-}][\mathrm{H_3O^-}]}{[\mathrm{CH_3COOH}]} \tag{2.1}$$

The pK_a of acetic acid in water equals 4.75. This indicates that acetic acid is a weak acid and acetic acid will be mostly present in the neutral form. Only the neutral form of acetic acid can be extracted into the organic phase, described by the distribution coefficient.

$$\mathrm{CH_3COOH_{aq} \rightleftarrows CH_3COOH_{org}}, \qquad K_\mathrm{d} = \frac{[\mathrm{CH_3COOH_{org}}]}{[\mathrm{CH_3COOH_{aq}}]} \tag{2.2}$$

The distribution coefficient (K_d, Eq. (2.2)) is the ratio between the acetic acid concentration in the two liquid phases at equilibrium, so it is dependent on the solubility of both phases. The theoretical value of K_d is 0.56 [17]. The partition coefficient (D, Eq. (2.3)) also takes the dissociated form of acetic acid into account.

$$D = \frac{[\mathrm{CH_3COO^-_{org}}] + [\mathrm{CH_3COOH_{org}}]}{[\mathrm{CH_3COO^-_{aq}}] + [\mathrm{CH_3COOH_{aq}}]} \tag{2.3}$$

As mentioned before, acetic acid is a weak acid and only the neutral form can be extracted towards the organic phase. Therefore, the partition coefficient is approximately equal to the distribution coefficient. Only the distribution coefficient will be further taken into account. The concentration can be determined by measuring the conductivity and calibrating it to the real concentration, which includes the dissociation.

2.2 Hydrodynamics

The forces acting on the to-be-dispersed phase can be most easily be analysed by a dimensionless analysis [18]. Dimensionless numbers compare different forces with each other based on the fluid properties, so the overruling force of the system can be determined. The flow patterns can be predicted with the knowledge about the forces from the dimensionless analysis [19]. The dimensionless numbers used are the Reynolds number (Re), Weber number (We), Bond number (Bo), and Capillary number (Ca). Eq. (2.4) is shown which forces are described by the dimensionless numbers and how they are calculated.

$$\mathrm{Re} = \frac{\text{inertial force}}{\text{viscous force}} = \frac{\rho u d}{\mu} \tag{2.4a}$$

$$\mathrm{Bo} = \frac{\text{gravitational force}}{\text{capillary forces}} = \frac{\rho g d^2}{\gamma} \tag{2.4b}$$

$$\mathrm{We} = \frac{\text{inertial force}}{\text{capillary forces}} = \frac{u^2 d \rho}{\gamma} \tag{2.4c}$$

$$\mathrm{Ca} = \frac{\text{viscous force}}{\text{capillary forces}} = \frac{\mu u}{\gamma} \tag{2.4d}$$

where ρ is the density of the dispersed phase in [kg/m^3], u the superficial velocity in [m/s], d the channel diameter in [m], μ the dispersed phase viscosity in [Pa.s], g the gravity force in [m/s^2], and γ the interfacial tension in [N/m^2] [20].

The Reynolds number is the ratio between inertial and viscous forces [20; 21]. A laminar flow is shown when $\mathrm{Re} < 2000$ and turbulent flow when $\mathrm{Re} > 4000$. The Stokes flow regime is usually the applicable regime for micro channels, since $\mathrm{Re} < 1$. The Bond number is the ratio between gravitational forces and interfacial tensions, or capillary forces. This number determines if the gravitational force plays any role in the process. The Weber number is the inertial force of the liquids compared to the capillary forces, which is a quantity used for the formation and breaking of droplets. The droplets become smaller with a higher Weber number. The capillary number gives an indication how the liquid behaves compared to the solid interface.

The forces of surface tension of a curved interface is exactly balanced by the difference in pressure on the two sides of the interface [9]. This is described by the Laplace equation, shown in Eq. (2.5).

$$P^\alpha - P^\beta = \frac{2\gamma}{r} \tag{2.5}$$

where P^α is the inside pressure, P^β is the outside pressure, γ the surface tension and r the radius. Eq. (2.5) holds for spherical interfaces. The difference in pressure ($P^\alpha - P^\beta$) is called the Laplace pressure.

2.2.1 Liquid-liquid flow patterns

In general, four different flow patterns can be distinguished: laminar, droplet, slug, and chaotic flow (shown in Figure 2.1) [2]. The shown flow pattern is dependent on the forces acting on the fluids, which are described in the dimensionless analysis.

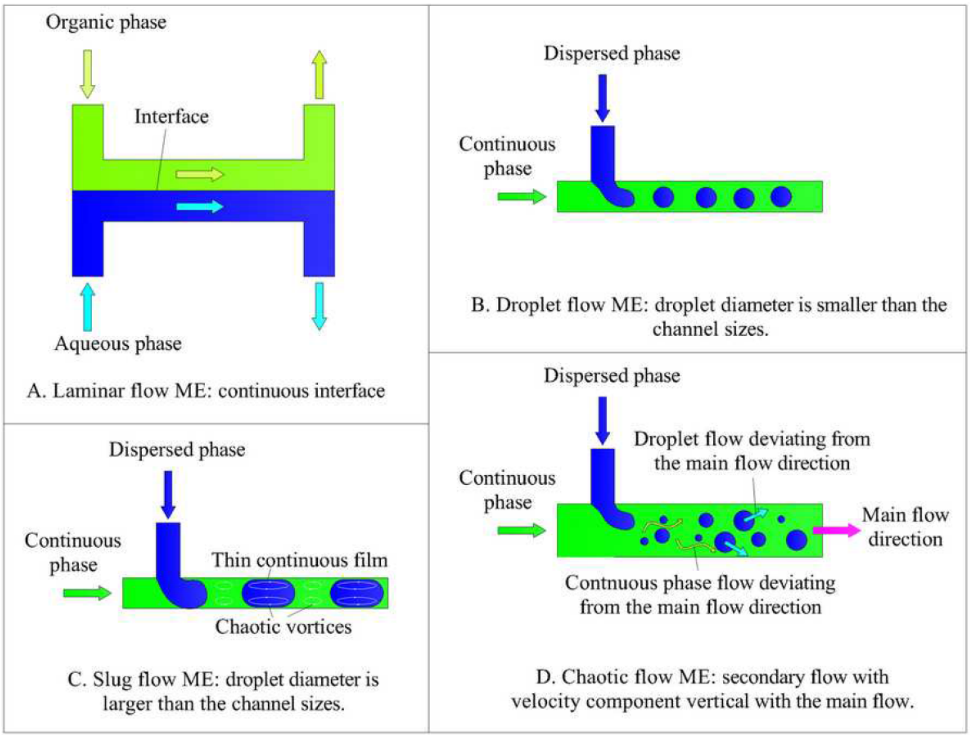

Figure 2.1: Most common flow patterns are laminar flow (A), droplet flow (B), slug flow (C), and chaotic flow (D), from [2] with permission from Elsevier.

Figure 2.1(A): Laminar flow In order to create a laminar flow, the viscous and inertial forces must be stronger than the interfacial force (We & Ca > 1) [3; 4]. Surface tension and friction forces dominate over gravity. The Laplace pressure is balanced with the pressure loss of both phases in order to get a stable flow [3]. The mass transfer is dominated by diffusion at the interface of two phases and can be described by the Fick's law of diffusion. The flow can be stabilized by, for example, increasing the velocities, addition of surfactants, and surface modification. Separation is easiest with an Y-shaped phase separator with different surface wettability.

Figure 2.1(B): Droplet flow Interfacial force is larger for droplet flow compared to the viscous and inertial forces (We & Ca < 1) [4]. The droplet diameter is smaller than the channel size, so there is no interaction of the dispersed phase with the wall. The advantage of droplet flow is the large interfacial area for mass transfer [2]. The main disadvantage is the more complicated separation compared to laminar flow [3]. An in-line Y-shaped phase separator with different wettability or out-line settler could be used as separation techniques [22].

Figure 2.1(C): Slug flow Droplet flow can be adjusted to slug flow by increasing the dispersed phase flux and decreasing the continuous phase flux [2]. The main difference between droplet and slug flow are the internal circulations which are present at slug flow [3]. Internal circulations are caused by the shear stress between the continuous liquid phase and the wall. Mass transfer is enhanced due to the internal circulation which causes faster surface renewal at the interface. The thin film layer between the slug and wall is determined by the wettability of the wall. Mac Giolla Eain et.al. (2013) found an expression for the wall film layer thickness, dependent on the Capillary and Weber number (Eq. (2.6)) [23].

$$\frac{h}{r} = 0.35(\mathrm{Ca})^{0.354}(\mathrm{We})^{0.097} \tag{2.6}$$

where h is the film thickness and r the radius of the capillary. The internal circulations are highly dependent on the wall film around the dispersed phase [24; 25]. The main advantage of the wall film is the enlarged interfacial area compared to slugs without wall film. The wall film has a low velocity due to the shear stress from the moving slug. Intensity of the internal circulations determine to which degree the convective mass transfer takes place, schematically shown in Figure 2.2.

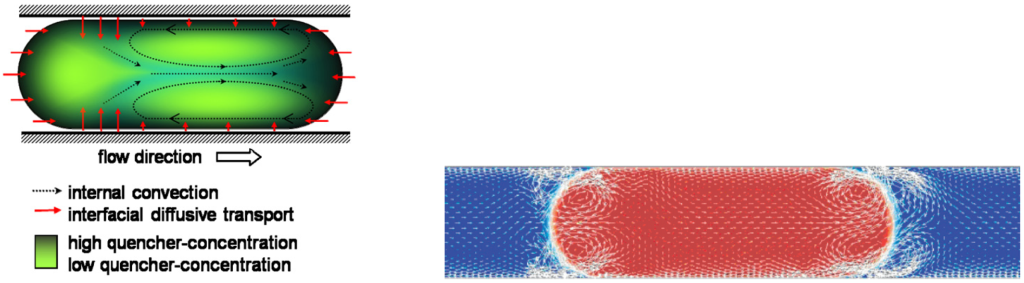

(a) (b)

Figure 2.2: Internal circulations for two phase slug flow. (a): Schematic of the acting forces on the slug. (b): slug circulations. Adapted from [24] with permission from Elsevier.

Two zones can be distinguished from Figure 2.2: stagnant and circulation zone [24]. The circulation zone is at the center of the slug. The velocity is effectively zero at the stagnant zones [25]. The zones are dependent on the viscosity and slug length and have a minimal dependency on slug velocity. The long slugs have multiple vortices with internal circulations, while short slugs are hardly influenced by the wall shear. Therefore, internal circulations are largest with larger slugs.

Figure 2.1(D): Chaotic flow In order to create a chaotic flow, extractors shaped as micromixers are needed [2]. Passive or active micromixers can be used, but passive micromixers are more common since active micromixers need an additional energy source. The main advantage of chaotic flow is that it is suitable for a high-throughput extraction. However, it is more complicated to control the exact flow patterns.

2.2.2 Gas-liquid-liquid flow patterns

Gas can be introduced in a liquid-liquid flow pattern in two ways, as is shown in Figure 2.3 [4]. In all cases, the liquids are not soluble in the gas slug.

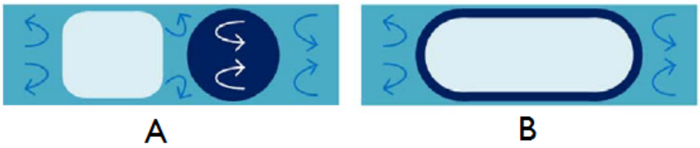

Figure 2.3: Two types of gas-liquid-liquid flow: slug flow with alternating gas-liquid slugs as dispersed phase (A) and double emulsion (B). Adapted from [4] with permission from Elsevier.

Figure 2.3(A) shows the gas phase dispersed in the continuous phase, creating alternating gas-liquid slugs. The gas phase is dispersed inside the dispersed liquid phase, creating a double emulsion in Figure 2.3(B). Both configurations increase the specific area between the dispersed and continuous phase, which increases the mass transfer. Mandalahalli (2015) modelled a double emulsion configuration where it was shown that the film layer around the gas slug is easily saturated [7]. The mass transfer was limited because the film layer could not be refreshed. There is only mass transfer in the front and end caps where also the internal slug circulations are the highest. The double slug flow does not have this problem, since the gas slugs do not have any mass transfer and the liquid slugs are not limited by a slug film layer. The internal circulations for the three phase double emulsion is shown in Figure 2.4.

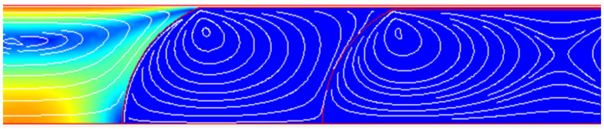

Figure 2.4: Internal circulations for three phase system: water, organic and gas (from left to right) with the velocity streamlines. Adapted from [7].

Figure 2.4 shows the velocity streamlines for water-octanol-gas system, which can be compared to the liquid-liquid velocity profile in Figure 2.2(b). It can be seen that the streamlines at the end of the slugs does not change with the additional gas.

2.3 Heterogeneous surface wettability

2.3.1 Flow Patterns

Surface heterogeneity can change the flow dynamics, depending on the applied pattern and process parameters. Meng et al. (2015) studied the effect of heterogeneous surface wettability and found four different results, passing, adhesion, phase inversion and breaking [8]. In order to understand what is happening during adhesion, phase inversion and breaking, one must understand the forces acting on the liquids and solid. The interface between liquids is formed due to the interfacial tensions, or Laplace pressure. The interfacial tension can be altered by surfactants. The solid-liquid interaction consists mainly of dipole-dipole interactions are known as van der Waals forces or dispersion forces. The final force is the convective force imposed by the pumps. Any imbalance between these forces can cause the effects shown in Figure 2.5.

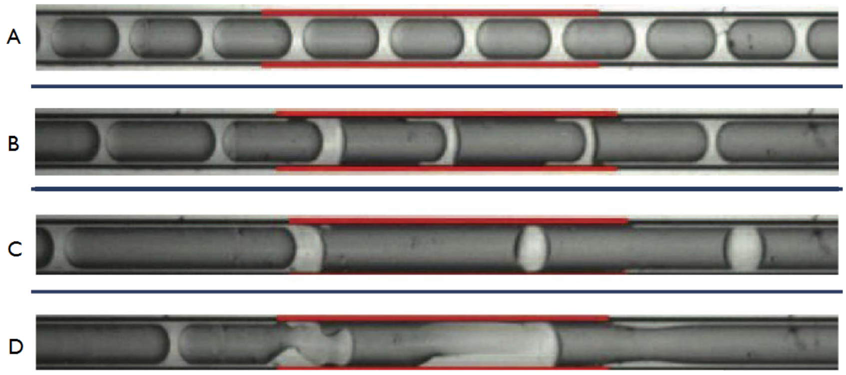

Figure 2.5: Different effects of heterogeneous surface wettability, capillary diameter of 580 µm with a patterning of 6 mm. (A): Passing. (B): Adhesion. (C): Phase inversion. (D): Breaking. Adapted from [8], with permission from Elsevier.

Passing When the slugs pass the patterning without modification, the convective force of the flow is too high. Also, the film thickness is too large for the van der Waals force to overcome [26].

Adhesion The forces are imbalanced when adhesion is shown. Energy of the film layer between the liquid slug and wall is overcome and the slug is chemically bonded to the wall (van der Waals force) [26]. It can be seen that the front cap of the slug is not altered, but the middle part and back cap are. The Laplace pressure at these points are smaller compared to the front cap. Therefore, disjoining pressure is strong enough to overcome the distance of film layer and rupture the liquid-liquid interface ($p_{\text{vdw}} = p_{\text{Laplace}}$).

Phase inversion Phase inversion occurs when the van der Waals force overcomes the Laplace pressure of the complete interface. The main difference with adhesion is that the front cap is also affected now, creating a complete inversion of dispersed and continuous phase at the hydrophobized part. Chen et.al. (2013) found an expression for the critical capillary number of phase inversion [26]. The critical capillary number is based on the dipole interactions and Laplace pressure, shown in Eq. (2.7).

$$\text{Ca}_{\text{critical}} = k\left(\frac{A}{\gamma d^2}\right)^{3/8}\left(\frac{D}{d}\right)^{3/4} \tag{2.7}$$

with k as fitting parameter, A is the Hamaker constant, γ the interfacial tension between the both liquid phases, d is the channel diameter, and D the slug length. The Hamaker constant is in the order of magnitude of 10^{-19} J and k was fitted at 2.5 for square channels.

Breaking Breaking occurs when the forces are out of balance, so it is accelerating and time-dependent. The convective flow is too high to form a new and stable flow.

2.3.2 Phase Inversion

Phase inversion can be predicted theoretically when the static contact angles are known. The contact angle in the capillary can be calculated by the force balance over the liquid-liquid interface at the wall in the capillary, shown in Figure 2.6 [9; 27].

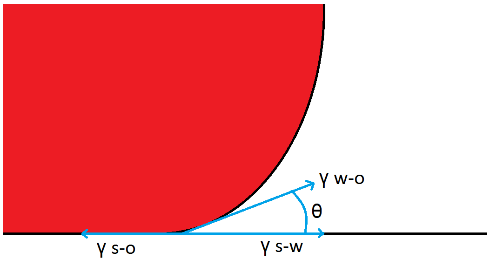

Figure 2.6: Schematic of the contact angle in the capillary with the different forces.

The contact angle can be calculated by making the force balance

$$\gamma^{\text{water-organic}}\cos\theta + \gamma^{\text{solid-water}} = \gamma^{\text{organic-solid}} \tag{2.8}$$

the forces γ^{sw} and γ^{so} can be calculated from the static contact angle with the following equations.

$$\gamma^{\text{organic}}\cos\theta_{\text{organic}} = \gamma^{\text{solid}} - \gamma^{\text{solid-organic}} \tag{2.9a}$$

$$\gamma^{\text{water}}\cos\theta_{\text{water}} = \gamma^{\text{solid}} - \gamma^{\text{solid-water}} \tag{2.9b}$$

The contact angle in the capillary can be calculated by combining Eq. (2.8), (2.9a) and (2.9b), resulting in the next equation.

$$\cos\theta = \frac{\gamma^{\text{water}}\cos\theta_{\text{water}} - \gamma^{\text{organic}}\cos\theta_{\text{organic}}}{\gamma^{\text{water-organic}}} \tag{2.10}$$

The equation above can be used for the hydrophobic and hydrophilic surface in order to predict the corresponding contact angle of the organic phase compared to the water phase. Contact line pinning occurs when the contact angle for the hydrophilic surface is higher compared to the hydrophobic surface [27]. With a pinning force present, the dispersed phase sticks to the wall surface. When the calculated contact angle is 0° or 180°, the corresponding phase completely wets the surface, forming a wall film around the other phase. The alternating contact angle could enhance the internal circulations. It is possible to model this prediction in COMSOL, which is done by J.A. Wood. The alternating contact angle is shown in Figure 2.7.

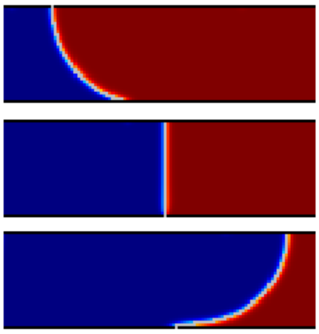

Figure 2.7: Shift in contact angle: Left wall is hydrophobic and right wall is hydrophilic. The red is water and blue is organic. The contact angle shifts when the organic phase moves towards the hydrophilic wall.

The contact angle shifts in Figure 2.7, which disturbs the internal circulations of the slug. Distortion of the slug should help increasing the mass transfer in the capillary.

2.4 Mass transfer performance

The mass transfer performance can be quantified by the extraction efficiency and the volumetric mass transfer coefficient [28]. The extraction efficiency gives an impression of how much mass is transferred from the aqueous to the organic phase (Eq. (2.11)). An extraction efficiency of 100% represents equilibrium between the phases.

$$E\ [\%] = \left(\frac{w_{\text{aq,in}} - w_{\text{aq,out}}}{w_{\text{aq,in}} - w^*_{\text{aq}}} \right) * 100\% \tag{2.11}$$

where $w_{\text{aq,in}}$ is the inlet weight fraction, $w_{\text{aq,out}}$ the outlet weight fraction and w^*_{aq} the equilibrium weight fraction. The volumetric mass transfer coefficient is derived from the total flux which can be achieved over time.

$$\frac{dw_{\text{aq}}}{dt} = -R_{\text{aq}}a = -k_{\text{L}}a(w_{\text{aq}} - w^*_{\text{aq}}) \tag{2.12}$$

In most literature, it is assumed that the aqueous concentration does not change significantly over time so $w_{\text{aq}} = w_{\text{aq,in}}$ over the whole length. The volumetric mass transfer coefficient can then be derived with the following boundary conditions. At the start of time ($t = 0$) the concentration is equal to the inlet concentration ($w_{\text{aq}} = w_{\text{aq,in}}$) and when the residence time is reached ($t = \tau$) the concentration is the outlet concentration ($w_{\text{aq}} = w_{\text{aq,out}}$). This results in the following equation.

$$k_{\text{L}}a = \frac{1}{\tau} \ln \left[\frac{w_{\text{aq,in}} - w^*_{\text{aq}}}{w_{\text{aq,out}} - w^*_{\text{aq}}} \right] \tag{2.13}$$

This equation is valid when the aqueous concentration does not change significantly over time. This research uses a diluted aqueous solution, so the previous equation may not be valid. Two balances are needed to overcome this limitation (shown in Eq. 2.14),

$$\epsilon_{\text{aq}} \frac{dw_{\text{aq}}}{dt} = -k_{\text{L}}a \left(\frac{w_{\text{aq}}}{K} - w_{\text{org}} \right) \tag{2.14a}$$

$$\epsilon_{\text{org}} \frac{dw_{\text{org}}}{dt} = k_{\text{L}}a \left(\frac{w_{\text{aq}}}{K} - w_{\text{org}} \right) \tag{2.14b}$$

In the equations above ϵ is the phase holdup defined as the ratio of the flow over the total flow ($\epsilon_{\text{n}} = Q_{\text{n}}/Q_{\text{tot}}$, with n = aqueous or organic) and K is the partition coefficient defined as $K = \frac{\rho_{\text{aq}}}{\rho_{\text{org}}} \frac{1}{K_{\text{d}}}$. The inlet conditions are defined as following:

$$w^{\text{in}}_{\text{aq}} \epsilon_{\text{aq}} = w_{\text{aq}} \epsilon_{\text{aq}} + w_{\text{org}} \epsilon_{\text{org}}, \qquad w^{\text{in}}_{\text{aq}} \epsilon_{\text{aq}} = w^*_{\text{aq}} \epsilon_{\text{aq}} + w^*_{\text{org}} \epsilon_{\text{org}} \tag{2.15}$$

Eq. (2.14) can be solved with the inlet conditions given in Eq. (2.15) and outlet conditions $w_{\mathrm{aq}} = w_{\mathrm{aq,out}}$ at $t = \tau$, which results in the final equation for the volumetric mass transfer coefficient.

$$k_{\mathrm{L}}a = \frac{1}{\tau\left(\frac{1}{K\epsilon_{\mathrm{aq}}} - \frac{1}{\epsilon_{\mathrm{org}}}\right)} \ln\left[\frac{w_{\mathrm{aq,in}} - w^*_{\mathrm{aq}}}{w_{\mathrm{aq,out}} - w^*_{\mathrm{aq}}}\right] \tag{2.16}$$

The interfacial area could be calculated and used in combination with the volumetric mass transfer coefficient to determine the mass transfer coefficient. The approach used to calculate this interfacial area is explained in Appendix B.

Error analysis The inlet concentration, outlet concentration and flows need to be measured to calculate the volumetric mass transfer coefficient and extraction efficiency. Several measuring errors can be detected and used to determine the error margins. A detailed study of the error analysis is performed and shown in Appendix C.

2.5 Research goals

From the literature study, some research goals can be set in order to answer the main question: *"What is the effect of heterogeneous surface wettability on the mixing patterns and resulting extraction in circular capillaries?"*

1. The operating parameters (extraction efficiency in case of ideal mixing, cleaning of the capillary, patterning method, etc.) should be studied in order to understand the process and ensure all experiments could be compared fairly.
2. Study the basic liquid-liquid and gas-liquid-liquid flow with homogeneous surface wettability.
3. Study the effect of heterogeneous surface wettability with different wettability lengths on the liquid-liquid and gas-liquid-liquid flows.

Chapter 3

Methods and Materials

The experimental part can roughly be divided in two subjects. The first is the part with homogeneous wetted capillaries in which liquid-liquid and gas-liquid-liquid experiments are performed as a reference for the heterogeneous wetted capillaries. The same liquid-liquid and gas-liquid-liquid extraction experiments are performed in the homogeneous and heterogeneous capillaries in order to get a fair comparison. This chapter firstly describes the experimental setup which is used during the extraction experiments. All the used materials (quantity and details) are listed in Appendix D.

3.1 Extraction setup

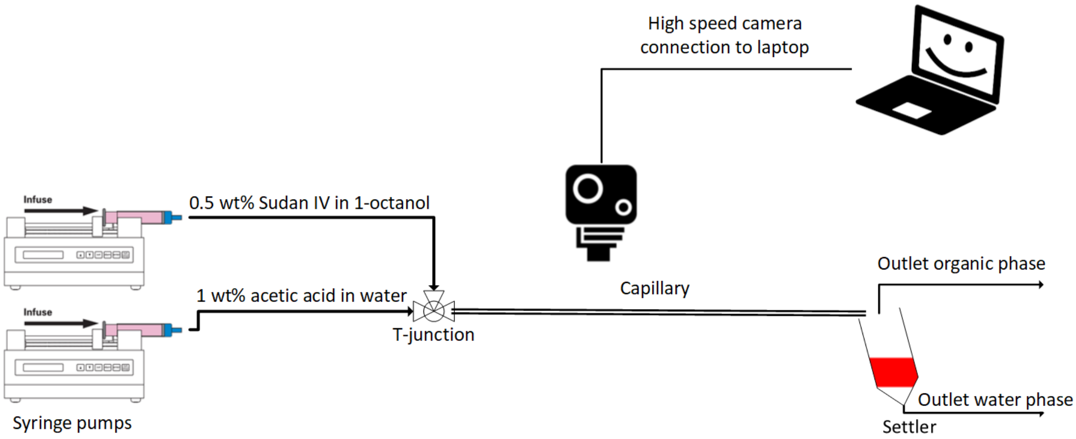

Figure 3.1: Schematical setup with two syringe pumps, the T-junction, capillary, settler and a high speed camera connected to a laptop.

The schematical setup is shown in Figure 3.1. Two syringe pumps are used to pump the solutions towards the capillary. One solution consists of 1 wt% acetic acid in MilliQ water, which is more pure compared to demineralized water. The other solution is 0.5 wt% Sudan IV in 1-octanol, which is filtered before usage. The Sudan IV dye is used to provide visual contrast between phases. Two 10 ml syringes with luer lock are used in the syringe pumps and connected to the capillary by a T-junction. The capillaries consist of borosilicate glass with a length of 150 mm, outer diameter of 1.5 mm and wall thickness of 0.225 mm. The effluent is captured in a home-made settler with a spout based on the siphon principle [16]. The water phase is collected by a syringe with needle via the spout. The collected water is stored in a plastic tube and diluted till 10 mL. The weight of the tube, collected and diluted water is measured to calculate the real effluent concentration. The electrical conductivity is measured three times to determine the effluent concentration. A calibration curve has been made in order to scale the electrical conductivity to the total acetic acid concentration (see Appendix E). Motion of the flow is captured with a high speed camera and a lamp is used to increase the contrast and for better illumination. The recording is saved as .Tiff images and analysed with ImageJ [29].

The gas-liquid-liquid experiments are conducted with the same setup. A cross-junction is used instead of the T-junction for the additional gas phase. The nitrogen gas is taken from the central network of the fumehoods. The nitrogen gas passes a dryer, pressure regulator, and mass flow controller before entering the capillary. A relief valve is installed for safety reasons. The nitrogen dryer is used to get the last impurities out of the nitrogen gas. The pressure regulator and mass flow controller are needed to get a stable flow. The mass flow controller works at pressures between 3 and 10 bar, so the pressure regulator is set at 3 bar.

3.2 Extraction experiments

The extraction experiments can be divided in two categories: two and three phase. The water flow rates are set in both categories. The two phase (liquid-liquid) experiments varies the ratio between the organic and water flow rate ($R = Q_{\text{org}}/Q_{\text{aq}}$), with a different total flow rate for each experiment. The three phase (gas-liquid-liquid) experiments have the water and total flow rate set, whereas the gas fraction varies and therefore, the organic to water ratio varies. In Figure 3.2 the set water flow rates, different organic to water ratios and gas fractions are shown.

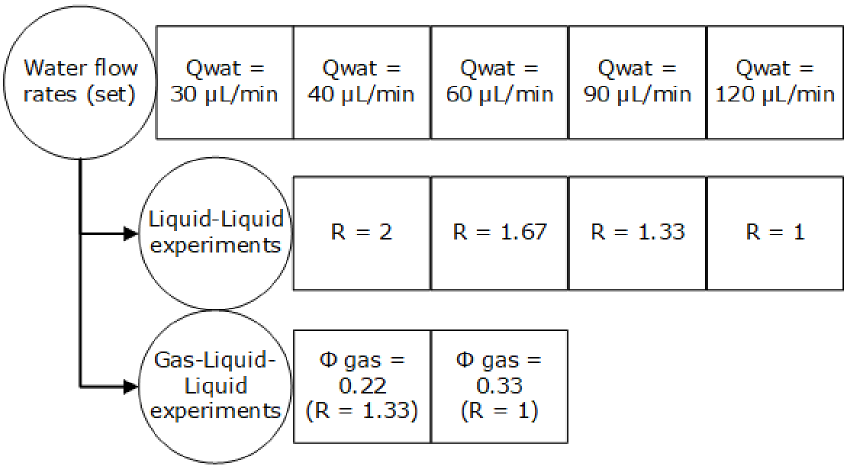

Figure 3.2: Experimental parameters which are changed during experiments.

Each experiment run is conducted in order to collect 1.5 mL of water phase, 50 minutes for the $Q_{\text{wat}} = 30$ µL/min and 13 minutes for $Q_{\text{wat}} = 120$ µL/min. Appendix E shows tables with the exact residence times and flow rates for each experiment.

3.3 Patterned hydrophobization

The hydrophobization starts with thorough cleaning of the capillaries in a cleanroom. The capillaries are flushed with 25 wt% potassium hydroxide at 75°C, then rinsed with MilliQ and placed for 10 minutes in an ultrasonic bath. Afterwards, the capillary is flushed again with MilliQ before being placed in 100% nitric acid for 10 minutes. After the nitric acid bath, the capillaries are flushed first with MilliQ and lastly with iso-propanol before drying them with nitrogen gas. The capillaries are further dried on a hot plate for an hour and stored in aluminium foil to prevent contaminations. This cleaning procedure will be called 'concentrated base/acid cleaning' from now on. The hydrophobization takes place after the cleaning in five different steps, illustrated in Figure 3.3.

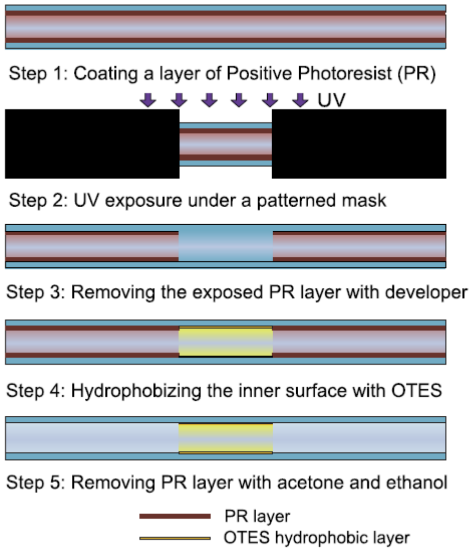

Figure 3.3: The five different steps of hydrophobization after cleaning. Adapted from [8] with permission from Elsevier.

The first three steps are executed in the cleanroom to make sure there are no contaminations in the capillary. The cleaning of the capillary is necessary for coating the inner capillary with a positive photoresist (PR) layer. A patterned mask is placed over the capillary, protecting the PR layer from ultraviolet light. The exposed parts of PR layer can be removed by a developer. A clearly shown pattern of unexposed PR layer remains in the capillary. For step 4, the hydrophobization, different methodologies are tried with different methods (gas or liquid hydrophobization), hydrophobization agents (Figure 3.4) and concentrations.

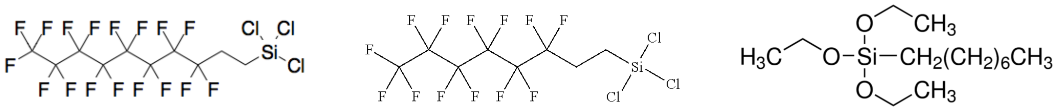

(a) FDTS (b) FOTS (c) OTES

Figure 3.4: Chemical structures of FDTS, FOTS and OTES.

In the gas method, dried nitrogen gas is pumped through the system. The hydrophobization agent is evaporated and carried by the nitrogen gas. In the liquid method, the hydrophobization agent is dissolved in a solvent and pumped through the capillary at 100°C. The gas method was investigated using FDTS or FOTS. However, the main disadvantage of FDTS and FOTS and the gas method is that it is very sensitive to environmental changes. Both crystallize very rapidly with water, so the system should be completely closed and dried properly. The gas method could be used, but due to the sensitivity to water it would be better to use the liquid method. The liquid method is tried with 3 v% FDTS in FC40 oil, 1 v% FDTS in hexane, 3 v% OTES in hexane, and 6 v% OTES in hexane. The FC40 oil is hard to remove from the capillary after hydrophobization since it does not dissolve in common solvents. Therefore, 3 v% FDTS in FC40 oil is not used as hydrophobization method. Both 1 v% FDTS and 3 v% OTES in hexane had the advantage that there were no oil residues in the capillary. However, the concentrations were too low making the hydrophobization not equally distributed over the capillary. FDTS was not further tried out since it polymerizes very rapidly with water. OTES does not polymerize that rapid, making it easier to work with. The 6 v% OTES hydrophobization resulted in a clean and stable flow, where phase inversion was shown.

Step 5, the hydrophobization, consists of 6 v% OTES dissolved in hexane pumped through the capillary for 2 hours at 20 µL/min in a dark room since light affects the PR layer. The photoresist layer (step 6) was removed with a 50/50 v%/v% mixture of acetone and ethanol, leaving a patterned capillary with alternating hydrophilic and hydrophobic parts.

Chapter 4

Operating Parameters

This chapter consists of some theoretical principles applied on the setup. Mainly models are described which have an influence on the performance of the extraction, like the T-junction determines the interfacial area. The main purpose of this chapter is to give a deeper insight in the experimental setup and which factors play a role during experiments.

4.1 Dimensionless analysis

The dimensionless numbers can be calculated with the information from Chapter 3. The gravitational force is 9.81 m/s^2, the channel hydraulic diameter is 10^{-3} m, and the highest superficial velocity is chosen, which is 8 mm/s. The density, viscosity and interfacial tension is given in the table below. Nitrogen gas density is calculated via the ideal gas law with 20 °C and atmospheric pressure. The gas viscosity is extracted from reference [30].

Table 4.1: Dimensionless analysis for all the different dispersed/continuous phase combinations.

	Octanol/Water	Water/Octanol	Gas/Octanol	Gas/Water
ρ [kg/m^3]	800	1000	$6.82 * 10^{-5}$	$6.82 * 10^{-5}$
μ [Pa.s]	$8.22 * 10^{-3}$	10^{-3}	$1.76 * 10^{-5}$	$1.76 * 10^{-5}$
γ [mN/m]	8.40	8.40	27.5	72.8
Re	0.818	8.40	$3.26 * 10^{-5}$	$3.26 * 10^{-5}$
Bo	1.03	1.29	$2.68 * 10^{-8}$	$1.01 * 10^{-8}$
We	0.80	1.00	$2.08 * 10^{-8}$	$7.87 * 10^{-9}$
Ca	$7.83 * 10^{-3}$	$9.53 * 10^{-4}$	$5.12 * 10^{-6}$	$1.93 * 10^{-6}$

In Table 4.1 it can be seen that the flow is laminar in all cases, as expected in a capillary. The Stokes flow regime is applicable when Re $<$ 1, which is for octanol in water and gas in liquid. The Bond number is the ratio between gravitational and capillary forces, which is approximately equal to each other for the liquid-liquid dispersed phases. Since the Weber and Capillary numbers are mostly lower than 1, it can be concluded that the capillary forces are dominant in all cases. Based on this analysis, slug flow is expected in the capillaries.

4.2 Phase Interactions

Different phase interactions are of importance in the extraction process. There are liquid-liquid, liquid-solid and gas-liquid interactions present in the experiments. The different interactions are studied by looking at the surface tensions, interfacial tensions and contact angles. The surface and interfacial tensions are determined with a drop shape analysis using Dataphysics OCA20 (contact angle meter). Figure 4.1 shows how the measurements are performed. The sessile drop method is used to determine the contact angle (Figure 4.1(a)) while pendant drop method is used for the interfacial and surface tension measurements, Figure 4.1(b) and (c) respectively.

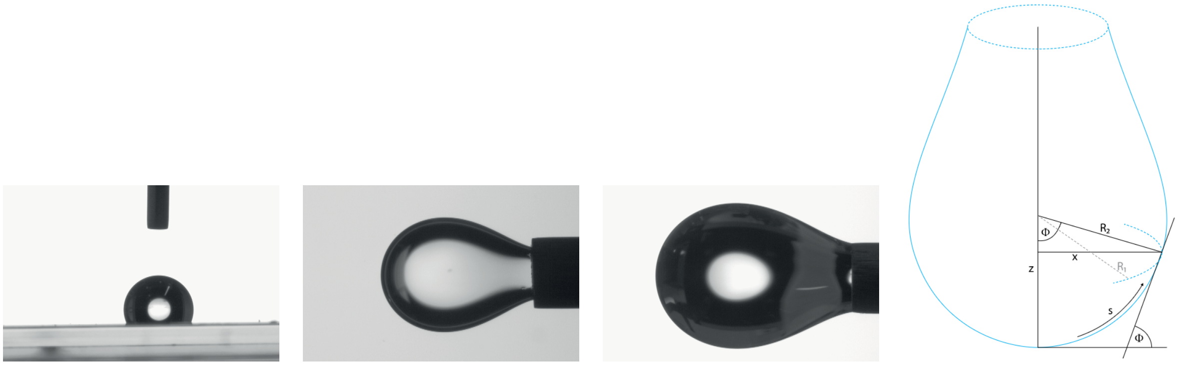

(a) (b) (c) (d)

Figure 4.1: Contact angle meter measurements. (a): Contact angle of 1 wt% acetic acid solution on FDTS hydrophobized glass slice. (b): Interfacial tension of 0.5 wt% acetic acid dispersed in 0.05 wt% Sudan IV. (c): Surface tension of MilliQ water. (d): Parameters in order to calculate the interfacial tension with the pendant drop method, adapted from [31].

The interfacial and surface tension are calculated with a set of differential equations, shown in Equation 4.1, which is a derivation of the Young-Laplace equation [31].

$$\frac{\mathrm{d}\phi}{\mathrm{d}s} = -\frac{\sin\phi}{x} + \frac{2}{r} \pm \frac{\Delta\rho g z}{\sigma}, \qquad \frac{\mathrm{d}x}{\mathrm{d}s} = \cos\phi, \qquad \frac{\mathrm{d}z}{\mathrm{d}s} = \sin\phi \tag{4.1}$$

where ϕ is the tangent angle, s is the arc length, σ the surface tension, and x and z the Cartesian coordinates (also shown in Figure 4.1d). The boundary condition for $s = 0$ is $z = 0, \phi = 0, r = 0$. The contact angle is simply measured by setting a baseline and measuring the angle between the baseline and droplet.

The error margin for these measurements is highly dependent on the contrast between the phases and quality of the picture. When a low resolution is used, it is harder make an estimation of the interfacial tension. The method works most accurate when the volume of the droplet is close to the critical volume, which is when the droplet falls [32].

4.2.1 Surface tension

The surface tension of both MilliQ and 1-octanol are measured. The acetic acid concentration in water is ranged up till 2 wt% and the Sudan IV concentration to 0.5 wt% in octanol. The results are shown in Figure 4.2.

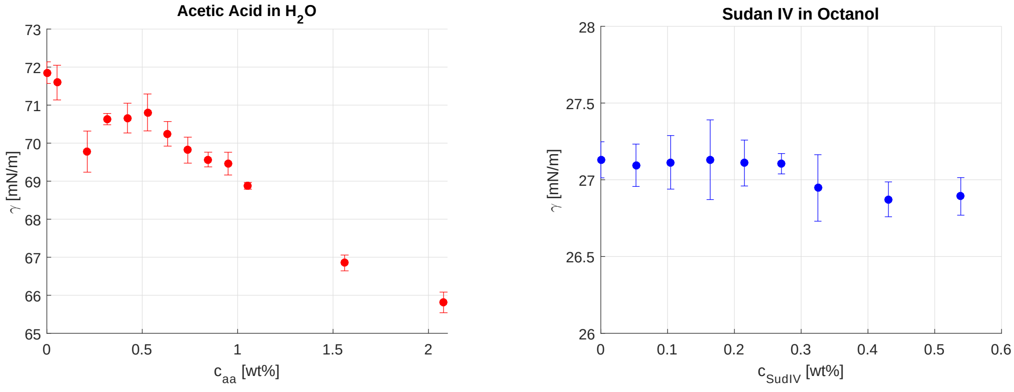

(a) (b)

Figure 4.2: Surface tensions for different concentrations of acetic acid in water (a) and Sudan IV in octanol (b). The error bars indicate the spreading between the measurements.

The surface tension of acetic acid decreases linearly with increasing concentration of acetic acid. Although it decreases linearly, there is no large difference in the initial concentration (1 wt% acetic acid, $\gamma \approx 70$ mN/m) and pure water ($\gamma = 72$ mN/m). The surface tension for water is 72.8 mN/m [9], so the surface tensions are a bit underestimated. The surface tension for octanol is approximately 27 mN/m, independent of the Sudan IV concentration, while the theoretical surface tension of pure octanol is 27.5 mN/m [33]. In conclusion it can be said that the acetic acid lowers the surface tension of water slightly, but without any real change. Sudan IV does not influence the surface tension of 1-octanol.

4.2.2 Interfacial tension

The interfacial tension between two phases is of importance for the extraction. If the interfacial tension increases, the mass transfer resistance for the extractant to the solvent increases and therefore, decreases the extraction efficiency [34]. The interfacial tensions of all different liquid-liquid combinations are shown in Table 4.2. The interfacial tension is measured with 0.05 wt% Sudan IV instead of 0.5 wt%, since the 0.5 wt% did not have a good contrast between the phases.

Table 4.2: Interfacial tensions between different liquid-liquid configurations measured with the pendant drop method.

Octanol	γ [mN/m] Pure octanol	γ [mN/m] 0.05 wt% Sudan IV
pure water (theory [9])	8.5	-
pure water	7.88 ± 0.01	7.85 ± 0.04
0.5 wt% AA	7.72 ± 0.03	7.45 ± 0.04
1 wt% AA	7.66 ± 0.05	7.53 ± 0.05
0.05 wt% Sudan IV + 1 wt% AA at equilibrium		8.08 ± 0.06

The pure phases have the highest interfacial tension. With the addition of more acetic acid, the interfacial tension decreases slightly. The Sudan IV decreases the interfacial tension only a really small amount, which is also expected from the measured surface tension. The results are consistent with the surface tension measurements, where the acetic acid decreased the surface tension and the effect of Sudan IV is negligible. The interfacial tension is a bit lower compared to the theoretical value, this was also shown for the surface tension.

4.2.3 Contact angle

The contact angle of MilliQ water, 1 wt% acetic acid in MilliQ water and 0.5 wt% Sudan IV in 1-octanol is measured on cleaned borosilicate glass and FDTS or OTES hydrophobized borosilicate glass. The borosilicate glass slices which are used are from a glass wafer with the most comparable material properties compared to the glass capillaries.

Table 4.3: Contact angle of MilliQ water, 1 wt% acetic acid in water and 0.5 wt% Sudan IV in 1-octanol on cleaned glass slices and hydrophobized glass slice with FDTS or OTES.

	Hydrophilic	Hydrophobic (FDTS)	Hydrophobic (OTES)
MilliQ water	Complete wetting	113.5° ± 0.6	74.6° ± 5.5
1 wt% Acetic Acid in water	12.1° ± 3.0	111.6° ± 1.4	-
0.5 wt% SudIV in octanol	24.1° ± 2.4	73.4° ± 1.0	30.7° ± 4.6

The contact angle of water on a clean surface is non existing, the water spreads all over the hydrophilic surface. With a small amount of acetic acid, there is a very small contact angle. The contact angle of octanol is only a bit larger compared to the acetic acid solution. This is due to the hydrophilic part of octanol, which causes the octanol to spread mostly over the surface. The hydrophobized slice gives high contact angles for both water and acetic acid, as expected. The octanol does not spread out on the hydrophobic surface like water on the hydrophilic surface. This is again due to the partly hydrophilic behaviour of octanol. The difference in contact angles on the FDTS and OTES hydrophobized slices is due to the different chemical structures of both. FDTS has many F-sidegroups while OTES consists of hydrocarbons. FDTS appears to be more hydrophobic since it repels water more strongly.

The contact angles are known, which means that the contact angle in the capillary could be measured, as described in Section 2.3.2. The following equation was derived:

$$\cos\theta = \frac{\gamma^{\text{water}}\cos\theta_{\text{water}} - \gamma^{\text{organic}}\cos\theta_{\text{organic}}}{\gamma^{\text{water-organic}}} \tag{4.2}$$

The contact angles of the FDTS and OTES hydrophobized glass slices are measured, which means that this can be compared to each other. the contact angle measured is from the octanol relative to the water.

Table 4.4: Contact angle of octanol relative to water for different hydrophobization agents: FDTS & OTES.

	FDTS	OTES
Hydrophilic	0°	0°
Hydrophobic	180°	125°

Contact line pinning occurs when the contact angle for the hydrophilic surface is higher compared to the hydrophobic surface, for a hydrophilic phase [27]. Therefore, the water should be the continuous phase for the hydrophilic parts and organic the continuous phase for the hydrophobic parts.

4.3 Cleaning of the capillary

The capillaries used for this research were stored for two years, in which contaminations build up inside the capillaries. The search for a proper cleaning method is essential in order to create stable flow inside the capillary during extraction experiments. The cleaning procedures are stated below.

1. Demineralized water and drying with nitrogen
2. Pure ethanol and drying with nitrogen
3. Diluted NaOH (1%) at 70°C for 1 hour, 5% HCl for 1 hour at 70°C and drying with nitrogen
4. Concentrated KOH (25%) at 75°C for 10s, rinse with water and sonicate for 10 minutes at 20°C, rinse with water, 100% HNO_3^- at 20°C for 10 min, rinse with water, rinse with isopropanol, dry with nitrogen and place on a hot plate for final drying.

Cleaning method 4 is also needed for the hydrophobization to make the PR layer stick properly to the capillary wall. All cleaning procedures are quantified by two methods: capillary rise [35] and contact angle, which are discussed in the following sections.

4.3.1 Capillary rise

The capillary rise experiment is done with MilliQ water. The theoretical capillary rise is determined by Eq. (4.3) [9]. The largest possible error is in the capillary diameter (0.05 mm), which is used for the error analysis.

$$h = \frac{2\gamma}{\rho g r_c}, \qquad \Delta h = \frac{2\gamma \Delta r_c}{\rho g r_c^2} \tag{4.3}$$

The capillary rise is measured directly after the cleaning procedure (rinse 0). The capillary is rinsed with water, dried with nitrogen gas and the capillary rise is measured again. This is done for four times for every capillary. The capillary rise versus the times rinsed is shown in Figure 4.3. The capillary rise is measured for two types of capillaries: old and new. The old capillaries are two years old and were stored in a closet. The new capillaries were ordered during the project.

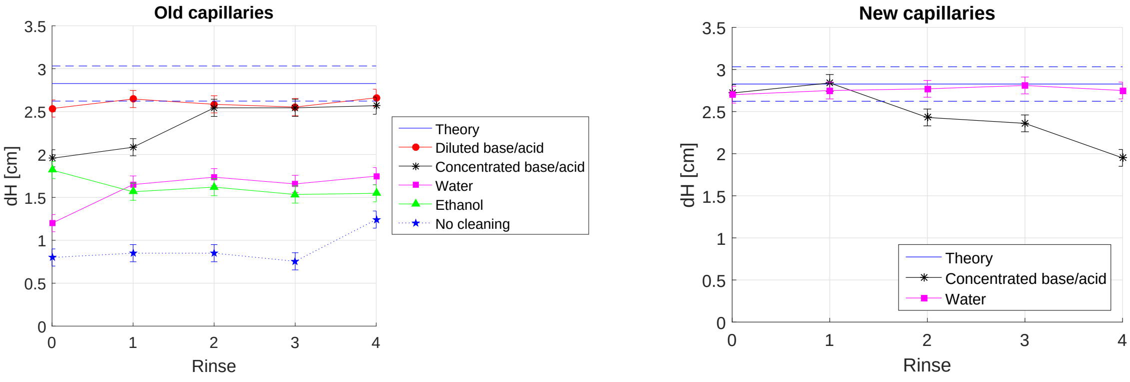

(a) (b)

Figure 4.3: Capillary rise for different cleaning methods before and after rinsing with water, (a): old capillaries, (b): new capillaries. The dotted lines indicate the error margin of the theoretical value.

Figure 4.3(a) shows that cleaning with only water or ethanol is not substantial enough to reach the theoretical capillary rise for the old capillaries. Cleaning with a base/acid combination gives the best result. The capillary rise for both cleaning procedures is comparable to the theoretical capillary rise. The diluted base/acid combination gives the most stable results closely to the theoretical value. The concentrated base/acid combination should be enriched with a water cleaning before usage to guarantee the same results as the diluted base/acid combination. The new capillaries do not need thorough cleaning before usage. Only water cleaning is enough to get the theoretical capillary rise.

4.3.2 Contact angle

The second experiment which is done to validate the cleaning procedures is a contact angle measurement of MilliQ water, acetic acid solution and Sudan IV in 1-octanol solution on a flat glass surface. The glass surface is made of comparable material with the capillaries i.e., borosilicate. The same cleaning procedures are applied on the glass surface as for the capillaries. The glass slices were stored with a clinging foil to prevent contaminations. The removal of the foil left a small amount of glue, making the surface contaminated. The results are shown in Table 4.5.

Table 4.5: Contact angle of MilliQ water, 1 wt% acetic acid in water and 0.5 wt% Sudan IV in 1-octanol on glass surfaces which are cleaned according to the four different cleaning procedures.

Cleaning procedure	MilliQ (°)	Acetic acid (°)	Sudan IV (°)
1. H_2O cleaning	23.7 ± 3.6	24.8 ± 6.3	23.0 ± 0.8
2. EtOH cleaning	9.66 ± 1.03	17.2 ± 5.7	25.2 ± 1.6
3. Diluted base/acid cleaning	16.8 ± 1.5	21.1 ± 3.0	21.5 ± 4.0
4. Concentrated base/acid cleaning	Complete wetting	12.1 ± 3.0	24.1 ± 2.4

The contact angle is the lowest for concentrated base and acid cleaning procedure and the highest for only water cleaning. The water cleaning was not able to remove this glue which caused the high contact angle. All the other cleaning procedures were able to remove more contaminations.

For the concentrated base/acid cleaning it was not possible to measure a contact angle since the MilliQ water spread over the surface. The contact angle of 1-octanol does not change for all the experiments due to the hydrophilic and hydrophobic part of octanol. The contact angle of water with 1 wt% acetic acid is comparable to water or within error margin. The concentration of acetic acid is too low to act as a surfactant and lower the contact angle. For the cleaning procedure where concentrated base and acid is used there was complete wetting for the MilliQ water, so no contact angle could be measured. Also, the difference between the water phases and 1-octanol is the biggest with the concentrated base/acid cleaning. Therefore, it can be concluded that the concentrated base/acid cleaning provides the best cleaning procedure to make the glass as hydrophilic as possible.

Conclusion

Four different cleaning procedures are performed on old and new capillaries and glass slices. It can be concluded that the old capillaries need extensive cleaning with concentrated potassium hydroxide and nitric acid, before the capillary rise was comparable to the theoretical capillary rise. The new capillaries do not need such extensive cleaning, only water cleaning is enough. The contact angle is measured on glass slices which are also cleaned according to the cleaning procedures. From this experiment it can be concluded that all possible contaminations can be removed with the concentrated base/acid cleaning in order to get complete wetting of the surface. The concentrated base/acid cleaning procedure will be used for all extraction experiments to ensure all contaminations are removed from the capillaries.

4.4 Extraction efficiency ideal mixing

The case of ideal mixing should be investigated in order to know what the maximum extraction efficiency could be in the capillary. The degree of mixing could be determined by comparing the ideal mixing, homogeneous and heterogeneous surface wettability extraction experiments. The organic and water phase are added to a beaker according to the given ratio, after which the solution is stirred for the corresponding residence time at 500 rpm. When the stirring is stopped, coalescence occurred rapidly, creating two phases again which could be separated and measured. The extraction efficiency and volumetric mass transfer are calculated according to the equations given in Chapter 2.4. The result is shown in Figure 4.4a.

Figure 4.4(a) shows that the maximum extraction efficiency could be around 70% when the amount of octanol is twice as that of water (R = 2). The extraction efficiency is between 60 and 70% for ratios higher than 1.33. When the amount of water and octanol is equal (R = 1), the extraction efficiency is approximately 50%. It can be seen that the extraction efficiency hardly increases with residence time. Figure 4.4(b) shows the residence time versus the volumetric mass transfer coefficient. The volumetric mass transfer decreases with increasing residence time, all within the error margin of each other. Only for equal amounts of water and organic it diverges, just as for the extraction efficiency, which indicates that this ratio is too low for high extraction efficiency.

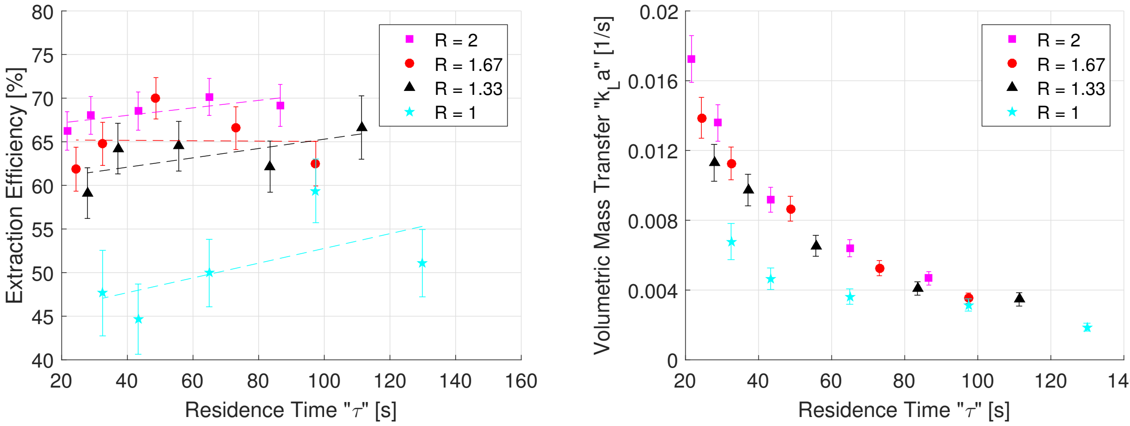

(a)

(b)

Figure 4.4: Results of the ideal mixing case. (a): Extraction efficiency. (b): Volumetric mass transfer.

4.5 T-junction

The T-junction is very important for the process since the two liquid flows are brought together here and the development of the flow starts here. Three different configurations are possible for the T-junction, which is shown in Figure 4.5 [36].

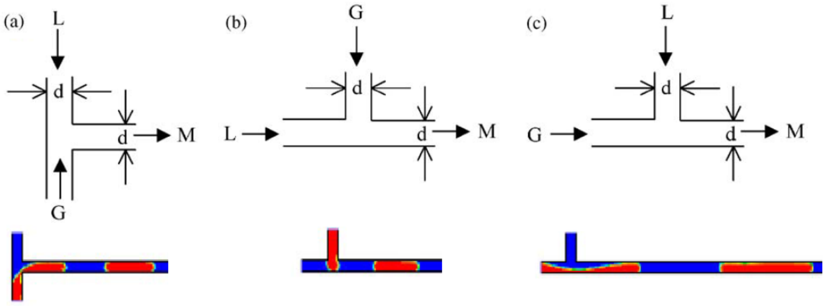

Figure 4.5: Three different configurations for a T-junction with their slug formations for a gas-liquid system, adapted from [36]. Configuration (a) & (b): Squeezing. Configuration (c): Jetting.

The configuration is important especially for the slug length. The squeezing configuration (Figure 4.5(a) and (b)) has two different mechanisms, dependent on the capillary number. For $\mathrm{Ca} > 10^{-2}$ slugs are formed due to a high shear stress. The slug length can be determined by a critical Weber number. For $\mathrm{Ca} < 10^{-2}$ the break up of slugs is caused by a capillary pressure imbalance at the droplet tail [4; 37]. In this case, the droplet length is mainly dependent on the flow rates of both phases (Eq. (4.4)).

$$\frac{L_\mathrm{d}}{w} = 1 + \beta \frac{Q_\mathrm{d}}{Q_\mathrm{c}} \tag{4.4}$$

where β is a fitting parameter in the order of magnitude of 1, w width of the channel, L_d slug length, Q_d and Q_c flow rates of the dispersed and continuous phase, respectively.

Figure 4.5(c) shows the jetting mechanism, where shear forces rupture the droplets under the resistance of capillary pressure [4]. This mechanism is dominated by the viscous and inertial forces, while the squeezing mechanism is dominated by the pressure drop. Both mechanisms are tried and the results are shown in Figure 4.6(a).

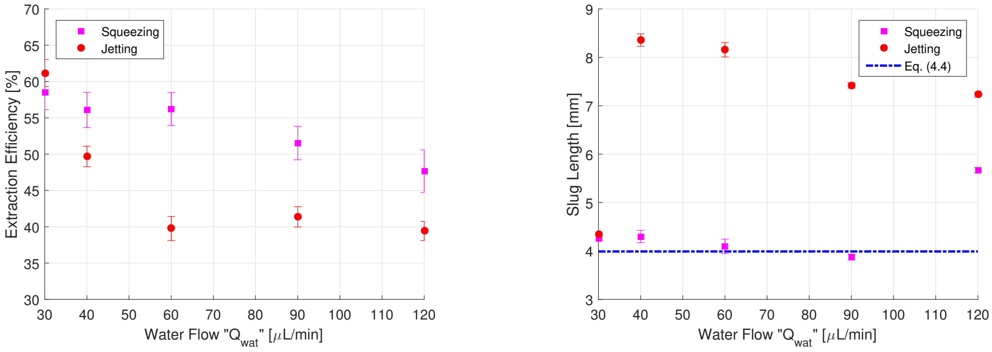

(a) (b)

Figure 4.6: The effect of the squeezing and jetting mechanisms with $Q_{org} : Q_{wat} = 2$. Extraction efficiency (a) and slug length (b) for different water flows.

From Figure 4.6(a) it can be seen that the extraction efficiency is higher for the squeezing configuration. In this configuration, the slug length is lower, so the specific area will be larger therefore higher extraction efficiency can be obtained. The jetting regime gives a much higher slug length, which results in a lower extraction efficiency. Eq. (4.4) is plotted for the slug length with fitting parameter (β) of 1.4. This equation fits the results for the squeezing regime nicely. There are two diverging results, which are for $Q_{wat} = 30$ µL/min for the jetting regime and for $Q_{wat} = 120$ µL/min of the squeezing regime. The first one gives slug length comparable to the squeezing configuration, with also a similar extraction efficiency. For the second one, there is a larger slug length then expected. Why these values differ so much is not known.

In conclusion, it is better to use the squeezing configuration since the slugs are smaller with this configuration. The smaller slugs result in higher interfacial area thus better mass transfer. Also, the internal circulations in the slug is mainly dependent on the slug size. The longer the slug, the higher the internal circulations. The slug size changes from 4.0 mm (for R = 2) to 2.5 mm (for R = 1), which will influence the internal circulations.

4.6 Separation

The two or three phases need to be separated at the end of the capillary. Different methods are tried to find the most easy and effective method. At first, the liquids were collected in a reaction tube. The different phases separated fast, but the organic phase always had to be removed first before the liquid phase could be collected. Secondly, a phase separator based on affinity was tried which is a T-shaped model with one outlet made out of stainless steel and the other of polychlorotrifluoroethylene (PCTFE) [22]. This should separate both phases instantly, but the used separator is designed for 3.2 mm diameter capillaries. Therefore, the phases did not get separated. Thirdly, a siphon based separator was made and tested, shown in Figure 4.7(a) [16]. The separator is essentially a settler for the phases and the main concern could be if there is mass transfer in the settler. Therefore, an experiment is conducted where the end of the capillary is imitated, but the two phases are directly poured into the settler. The fluids have the same residence time and contact in the settler as with an extraction experiment. The extraction efficiency is shown in Figure 4.7(b).

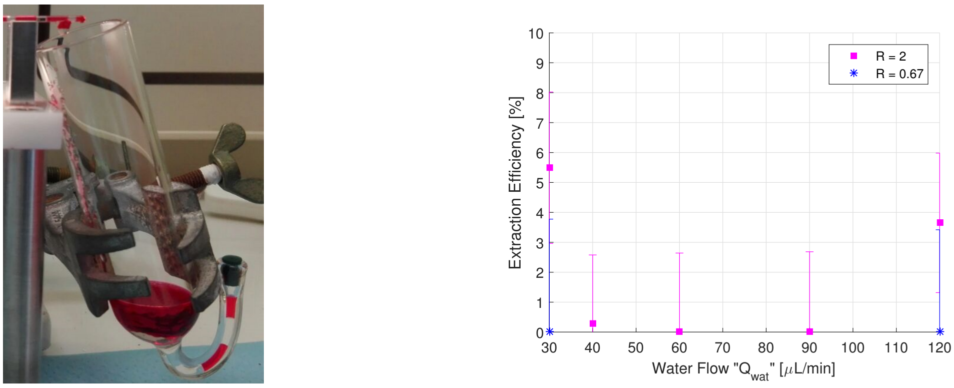

(a)

(b)

Figure 4.7: (a): Settler which is used for the experiments. (b): Result of the extraction experiments performed directly into the settler.

Figure 4.7(b) shows that there is hardly any extraction in the settler. It can be concluded that the settler works and it gives a good separation between the phases. The water phase can be easily separated from the organic phase and there is almost no mass transfer between the phases being separated.

4.7 Pressure drop

The pressure drop is the energy which is lost over the distance the liquid is transported, so it is the energy requirement of the pumps [1]. One phase flow pressure drop can be described by the Hagen-Poisseuille equation, which accounts for the frictional pressure drop [38]. Calculating the pressure drop is more complicated for two phase slug flow. The pressure drop is highly dependent on the slug size and inertia must not play any role in the flow (low Weber number) [39]. There are three different contributions to the pressure drop: frictional pressure drop of the dispersed and continuous phase, and the interfacial pressure. The frictional pressure drop can be described by the Hagen-Poisseuille equation, but is adjusted for the dispersed and continuous phase. The final contribution to the pressure drop is the interfacial pressure. Kashid et.al. (2007) used the Laplace pressure to calculate this contribution and proposed a model for the frictional contributions [38]. Jovanović et.al. (2010) refuted this method because it overestimates the interfacial pressure contribution for three reasons: it does not take the difference in contact angle into account, the contributions of the slug caps are summed up, and the superficial velocity of the continuous phase was taken into account for the frictional pressure [39]. Jovanović et.al. proposed two different models, stagnant film layer model and moving film model. They concluded that the film velocity is negligible, making the stagnant film layer model most appropriate. The model resulted in the following equation for the frictional pressure of the dispersed phase.

$$\Delta P_{\text{dispersed}} = \frac{8 u_{\text{slug}} \mu_{\text{d}} \alpha L}{(r-h)^2} \tag{4.5}$$

where u_{slug} is the slug velocity, μ_{d} viscosity of the dispersed phase, α slug length over the total unit cell length ($\alpha = l_{\text{d}}/(l_{\text{d}} + l_{\text{c}})$), L channel length, r channel radius, and h the film thickness. A similar equation is used to describe the frictional pressure drop for the continuous phase.

$$\Delta P_{\text{continuous}} = \frac{8 u_{\text{slug}} \mu_{\text{c}} \alpha L}{r^2} \tag{4.6}$$

The interfacial pressure is dependent on the channel length, unit cell length, Capillary number, interfacial tension, and channel diameter.

$$\Delta P_{\text{interfacial}} = \frac{L}{l_{\text{u}}} 7.16 \left(3\text{Ca}\right)^{2/3} \frac{\gamma}{d} \tag{4.7}$$

The total pressure drop for two phase slug flow is the summation of all three contributions. The pressure drop is estimated between 25 and 110 Pa for the performed two phase extraction experiments.

Ladosz et.al. (2016) proposed a pressure drop model for three (gas-liquid-liquid) phase flows in round microchannels [40]. The additional phase results in additional contributions for the pressure drop. An additional term for the interfacial pressure of the gas phase needs to be added. It gets complicated, since the velocity of the gas phase should be used (analog to Eq. (4.5) for the liquid dispersed phase) but the gas velocity is not constant. The gas slug expands with decreasing pressure, described by the ideal gas law.

The pressure drop is an important process parameter in case of scaling up the process. In this report, scaling up the process is not taken into account. Therefore, the pressure drop is not taken into account in further results.

4.8 Conclusions

The most important conclusions from this chapter are listed below.

- The addition of acetic acid or Sudan IV does not significantly change the interfacial tension over the system.
- The contact angles were used for a contact angle analysis where it was concluded that phase inversion is possible for the heterogeneous wetted capillaries.
- Slug flow is expected for all experiments, based on the dimensionless analysis.
- Cleaning of the capillary should be done with an extensive cleaning procedure with concentrated base and acid.
- The extraction is limited by the amount of organic compared to water, since the ideal mixing does not achieve 100% extraction.
- The most optimal configuration for the T-junction is the squeezing configuration since it gives the smallest slugs, thus highest interfacial area.
- Separation is possible by a gravitational settler without significant additional mass transfer.
- The pressure drop in the system is very small for liquid-liquid flows so it can be neglected.

Chapter 5

Two Phase Extraction

5.1 Homogeneous hydrophilic wetted capillary

Homogeneous hydrophilic capillaries are used in order to see which extraction efficiency could be achieved. Extraction experiments are performed for four different organic to water ratios, ranging from 2 to 1. The extraction efficiency and volumetric mass transfer coefficient are calculated according to the equations shown in Section 2.4. The results are shown in Figure 5.1.

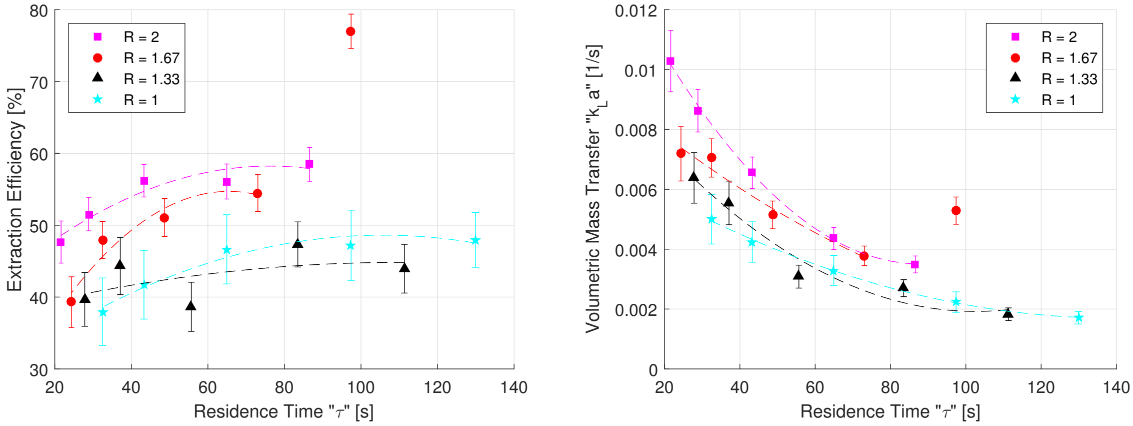

(a) (b)

Figure 5.1: Experimental results in the case of a hydrophilic capillary for different organic to water ratios and residence times. (a): Extraction efficiency. (b): Volumetric mass transfer coefficient. The lines are illustrative only.

The extraction efficiency increases with increasing ratio of organic versus water flow. The extraction efficiency varies roughly from 35 to 60%. There is an increase of approximately 10% in extraction efficiency for R = 2 and R = 1.67. There is no significant change over residence time for the lower ratios. The volumetric mass transfer coefficient was also calculated and shown in Figure 5.1(b), which decreases with increasing residence time and decreasing organic to water ratio. There is one outliner for R = 1.67 and $\tau = 100$s, probably due to a measuring error during the experiment.

The interfacial area is calculated for each experiment, the approach is shown in Appendix B.

The mass transfer can be calculated with the volumetric mass transfer coefficient and interfacial area. The interfacial area and mass transfer coefficient are shown in Figure 5.2.

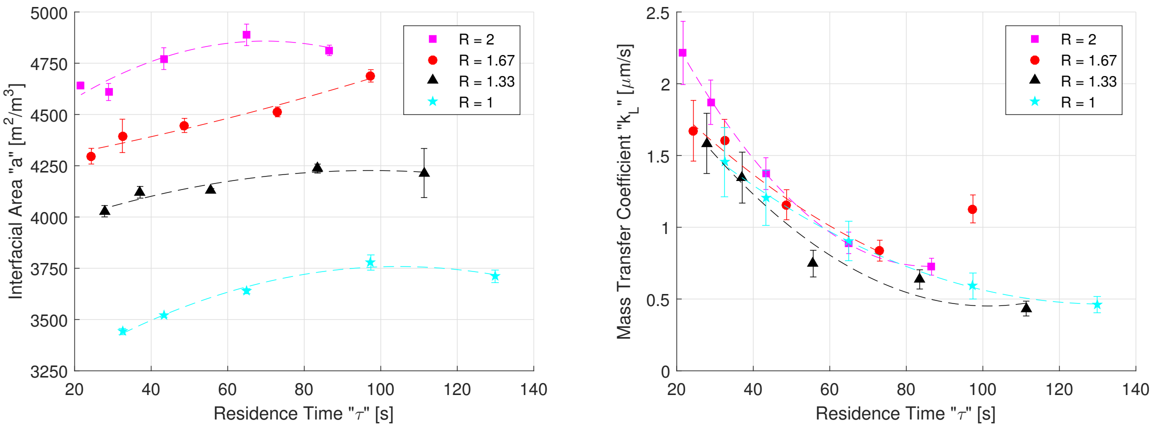

(a) (b)

Figure 5.2: The interfacial area (a) and mass transfer coefficient (b) for a homogeneous hydrophilic capillary, with different organic to water ratios. The lines are illustrative only.

Figure 5.2(a) shows the interfacial area versus the residence time. The slug size enlarges with higher organic to water ratios (Eq. (4.4)) and the distance between two slugs is relatively short for R = 2 compared to R = 1, since R = 1 relatively has double the amount of water. Therefore, the interfacial area is higher for higher organic to water ratios. The interfacial area increases approximately 250 m^2/m^3 with increasing residence time. Figure 5.2(b) shows mass transfer coefficient. The mass transfer decreases with increasing residence time, since it is proportional to the superficial velocity of the slug (see Appendix F). The organic to water ratio does not affect the mass transfer, since it was made independent of volumetric aspect.

Conclusion The homogeneous hydrophilic capillary was tested with different organic to water ratios over different residence times. The extraction efficiency increases with residence time and ratio, whilst the volumetric mass transfer coefficient decreases with the residence time. The interfacial area is between 3500 and 5000 m^2/m^3, with more interfacial area for higher amount of organic phase. The mass transfer coefficient is independent of the volume and decreases with residence time, proportional to the superficial velocity.

5.2 Heterogeneous wetted capillary

5.2.1 Flow patterns

The flow patterns shown in the capillary were also described in Chapter 2.3.1. Two different patterning lengths are experimented with: 1.0 and 6.0 mm. Four different flow patterns could be distinguished: passing, adhesion, phase inversion and breaking. Phase inversion is shown in Figure 5.3, adhesion in Figure 5.4(a) and passing in Figure 5.4(b). Break up of the flow was not observed during experiments.

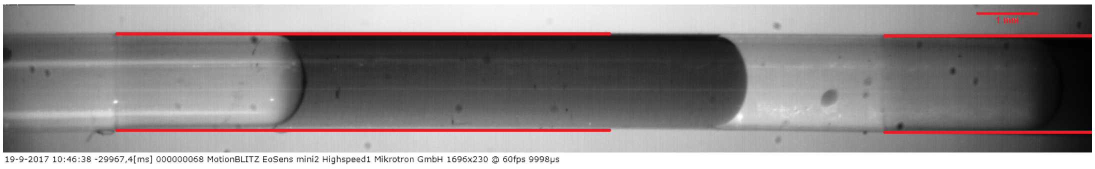

(a) $t = 0s$

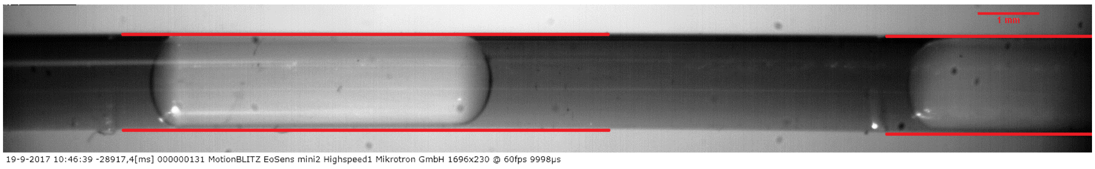

(b) $t = 1.17s$

Figure 5.3: Phase inversion observed for Q_{org} = 80 µL/min and Q_{wat} = 60 µL/min and patterning of 6.0 mm length, (a) on t = 0s and (b) on t = 1.17s. The red lines indicate the hydrophobized part of the capillary and the scale bar is for 1.0 mm.

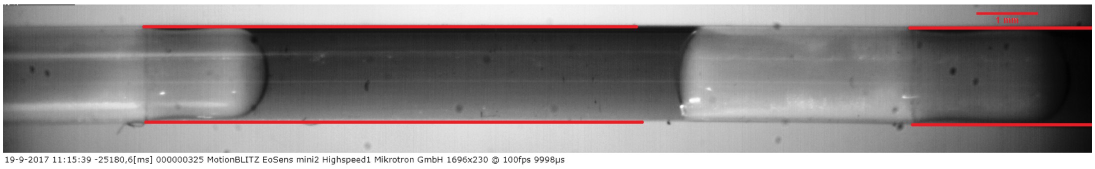

(a) Adhesion

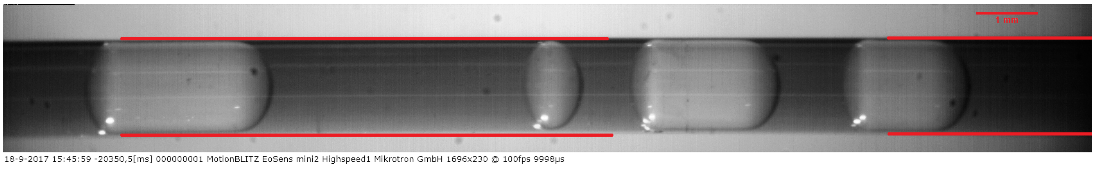

(b) Passing

Figure 5.4: Observation of (a) Adhesion, for Q_{wat} = 90 µL/min and Q_{org} = 120 µL/min. Passing (b), for Q_{wat} = 120 µL/min and Q_{org} = 200 µL/min and patterning of 6.0 mm length. The red lines indicate the hydrophobized part of the capillary and the scale bar is for 1 mm.

The patterning length in all cases should be 6.0 mm. However, the measured patterning length is ≈ 7.5mm. The increase in patterning length is due to the light scattering during the UV exposure under a patterning mask step in the hydrophobization. Figure 5.3 shows the 6.0 mm heterogeneous wetted capillary at two different time stamps. Figure 5.3(a) shows an organic slug with the left cap in the hydrophobic section and right cap in the hydrophilic section. The contact angle is approximately 28° of the organic slug in the hydrophilic part, whilst the water cap in the hydrophobic part has a contact angle of 25°. In Figure 5.3(b) the organic part has reached the hydrophobic sections, where it inverts from the dispersed to the continuous phase. Both water slugs are in the hydrophobic section where octanol is the continuous phase. For phase inversion, adhesion has to occur for the complete slug. In this case, adhesion means that the energy barrier of the film layer is overcome by energy of the wall. The energy barrier of the front cap is too high for adhesion. This can be seen in Figure 5.4(a), where the organic slug has a different orientation compared to the phase inversion at the same moment. Figure 5.4(b) shows water as the dispersed phase with irregular slug sizes. Water adhered to the hydrophilic part of the glass, breaking up the water slugs into smaller slugs. In the case of passing, the superficial velocity is too high in order for the slug to adhere to the surface. Since octanol has more affinity with the hydrophilic surface (contact angle of 24°) than water to the hydrophobic surface (contact angle of 75°), the continuous phase becomes octanol. Figure 5.5 shows the different flow patterns for all the extraction experiments.

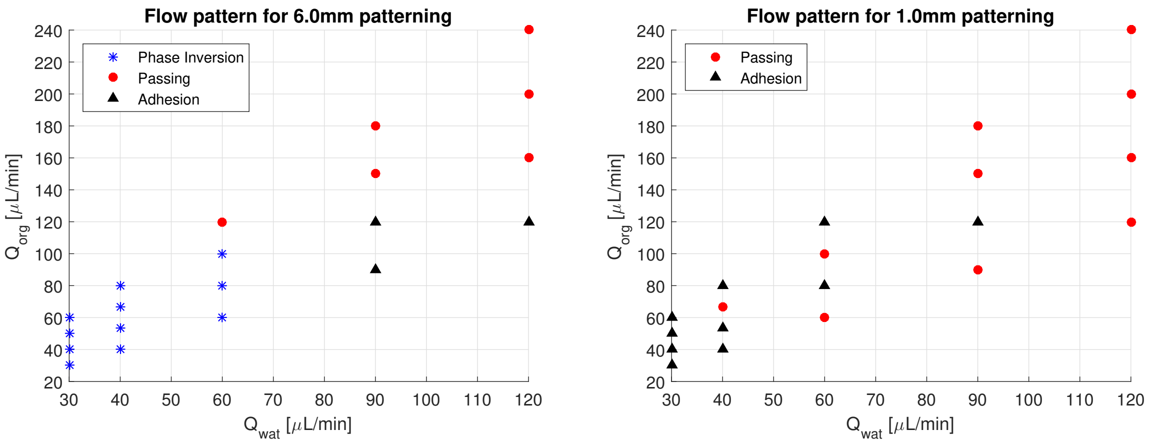

(a) (b)

Figure 5.5: The effect of heterogeneous surface wettability for different flow rates and flow ratios.

Figure 5.5(a) shows phase inversion, adhesion and passing for the 6.0 mm heterogeneous wetted capillary. Phase inversion occurs with the lower flow rates up to water flows of 60 µL/min. For the higher flow rates, there is no interaction with the wall any more (passing) or only by the film layer (adhesion). A similar trend was expected for the 1.0 mm heterogeneous wetted capillary, adhesion was expected instead of phase inversion. Figure 5.5(a) and (b) can be compared to each other, where it can be seen that not all results comply with each other. For example, for Q_{wat} = 60 µL/min and Q_{org} = 120 µL/min passing is shown for 6.0mm patterning and adhesion for 1.0mm patterning. In general, passing occurs for more flow rates and ratios with 1.0 mm compared to the 6.0 mm patterning. For the ratios R = 1.67 and 1 holds that the other experiments (R = 2 and 1.33 respectively) were done first, which gives the water time to adhere to the wall. Water adhered to the surface over time, making it impossible for the passing water slug with organic film layer to be brought into contact with the hydrophilic surface. Therefore, adhesion of the water slug can not take place at the hydrophilic surface.

The critical capillary number can be calculated, using the theory of Chen et.al. [26] (see Chapter 2.3.1). The critical capillary number should indicate when phase inversion or adhesion takes place in the capillary. Eq. (2.7) is shown here again.

$$Ca_{\text{critical}} = k\left(\frac{A}{\gamma d^2}\right)^{3/8}\left(\frac{D}{d}\right)^{3/4} \tag{5.1}$$

The constant k can be determined the slope of $\mathrm{Ca}\cdot d^{3/4}$ versus $(D/d)^{3/4}$, which is shown in Figure 5.6(a). The passing, phase inversion and adhesion are plotted for 1.0 and 6.0 mm heterogeneous patterning.

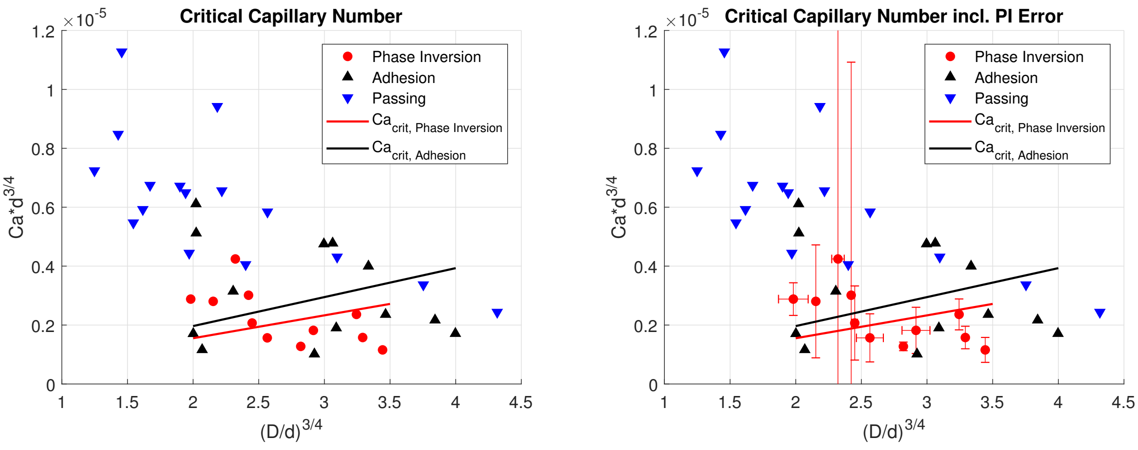

(a) (b)

Figure 5.6: Critical capillary number calculations with phase inversion, adhesion and passing plotted as different points. Eq. (2.7) is plotted for adhesion (black line) and phase inversion (red line). As illustration of the fitting accuracy, the errorbars of the x and y axis are also drawn for phase inversion in (b), illustrative for all points.

Figure 5.6(a) shows a large variation due to the different slug sizes (d). Eq.(2.7) was fitted for both the adhesion and phase inversion. The best fit would be a downward line, but both lines are upward due to the equation. Errorbars are included in Figure 5.6(b) to show the accuracy. The fitting parameter k is fitted with an 95% reliability interval, resulting in $k_{\text{phase inversion}} = 1.66 \pm 0.64$ and $k_{\text{adhesion}} = 2.09 \pm 0.88$. The goal of critical Capillary number is to predict the phase inversion. However, the fitting parameter for adhesion and phase inversion overlap each other when the error margins are taken into account. It can be concluded that the model provided by Chen et.al. is not sufficient for these experiments. For example, it does not include the patterning length.

Conclusion The flow patterns described in literature [8] are also observed for the two phase extraction experiments with 1.0 and 6.0 mm heterogeneous surface wettability. Passing, adhesion and phase inversion occurred for the 6.0 mm patterned capillaries whilst only passing and adhesion were observed for the 1.0 mm patterning. Breaking was not observed for any of the experiments. The critical Capillary number, which can be used to predict if phase inversion or adhesion is going to occur, was fitted for phase inversion and adhesion. The fitting parameter is $k_{\text{phase inversion}} = 1.66 \pm 0.64$ and $k_{\text{adhesion}} = 2.09 \pm 0.88$.

5.2.2 Extraction results

The extraction efficiencies of the 1.0 and 6.0 mm heterogeneous wetted capillary are shown in Figure 5.7.

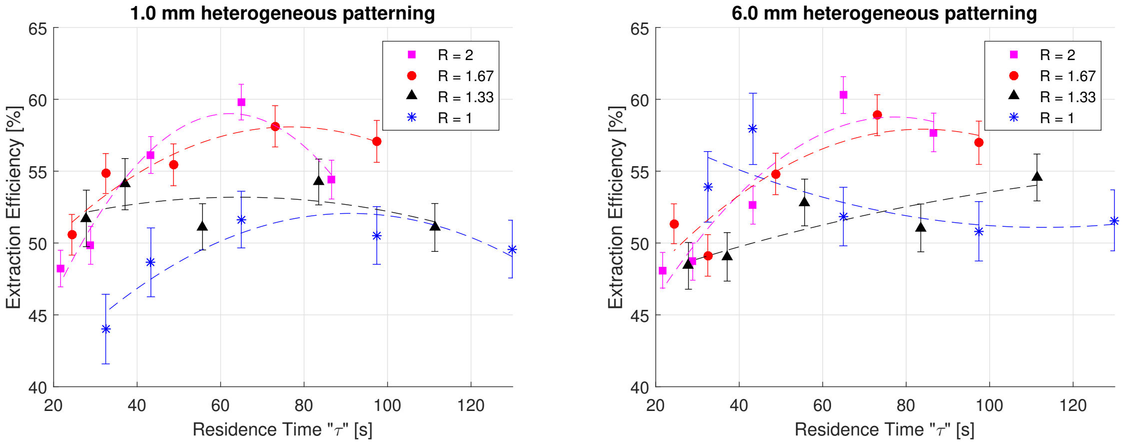

(a) (b)

Figure 5.7: Extraction efficiency for 1.0 mm and 6.0 mm patterning for different organic to water ratios. The lines are illustrative.

The extraction efficiency reaches a plateau, as can be seen for the ratios 1 and 1.67. Thus, the maximum extraction efficiency possible could be reached in the heterogeneous patterned capillaries. The highest extraction efficiency (≈ 60%) was achieved with the ratios 2 and 1.67 at the residence time of ≈ 70 seconds for both patterning lengths. For the 1.0 mm patterning it can be seen that the extraction efficiency does not change over the residence time for the ratio 1.33. In the case of ideal mixing it was already shown that the maximum achievable extraction efficiency is lowest for R = 1, which is also the case for 1.0 mm patterning. For 6.0 mm patterning, the extraction efficiency is very high for the lower residence times and R = 1, which are most likely outliers. The most optimal amount of organic appears to be 1.67 times the water since the extraction efficiency overlies the extraction efficiency of R = 2 for both patterning lengths. Next, the volumetric mass transfer coefficients for each organic to water ratio is compared for four cases: ideal mixing, 1.0 mm heterogeneous, 6.0 mm heterogeneous and homogeneous capillary. The results are shown in Figure 5.8 and 5.9.

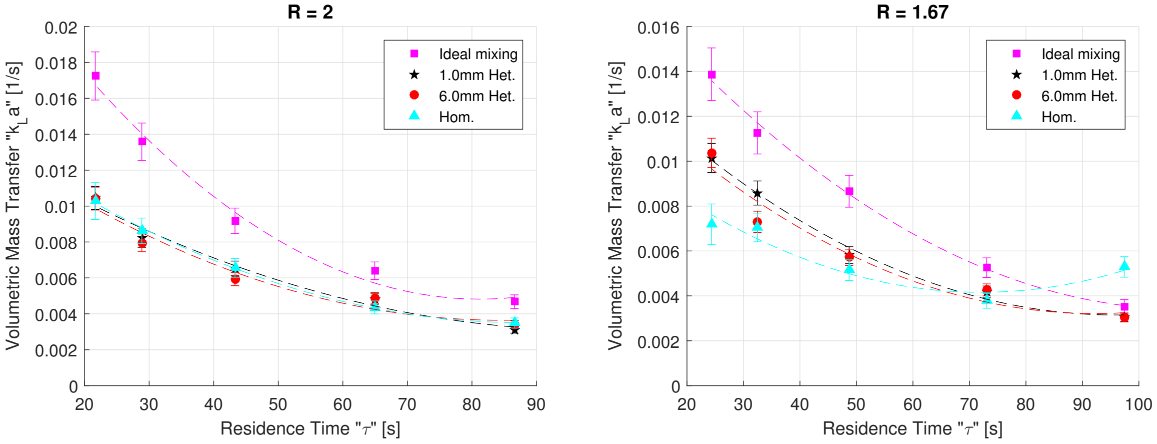

(a) (b)

Figure 5.8: Volumetric mass transfer coefficient in case of ideal mixing, heterogeneous capillary with the different patterning lengths and the base case, a completely hydrophilic capillary. The lines are illustrative.

The internal slug circulations are highest with the highest organic to water ratio. Figure 5.8(a) shows no elevation in volumetric mass transfer for the patterned capillaries compared to the hydrophilic capillary. The volumetric mass transfer coefficient in case of ideal mixing is higher, which means there is another mass transfer limitation. For R = 1.67 (Figure 5.8(b)) there is an increase in volumetric mass transfer compared to the homogeneous capillary, but the ideal mixing is not achieved.

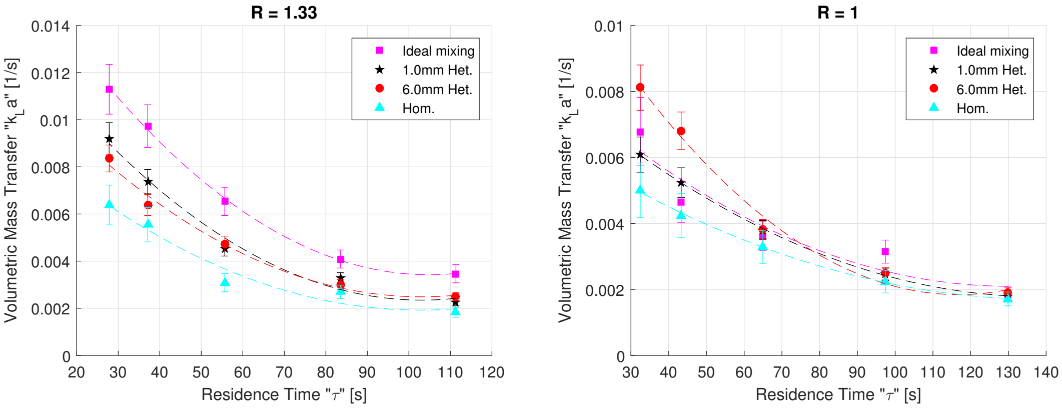

(a) (b)

Figure 5.9: Volumetric mass transfer coefficient in case of ideal mixing, heterogeneous wetted capillary with the different patterning lengths and the base case, a completely hydrophilic capillary. The lines are illustrative.

The lower organic to water ratios do have an increase in volumetric mass transfer coefficient for the heterogeneous capillaries (Figure 5.9). However, ideal mixing mass transfer is reached only for R = 1. The mass transfer of the homogeneous capillary also lies closest to the ideal mixing efficiency in this case. The volumetric mass transfer is not influenced by the patterning lengths since the volumetric mass transfer coefficients of 1.0 and 6.0 mm patterned capillaries are always close to each other. It can be concluded that the enhancement by heterogeneous wetted wall is largest when the amount of organic and water is equal to each other and there is 6.0 mm patterning. Figure 5.10 shows how it compares with the homogeneous capillary.

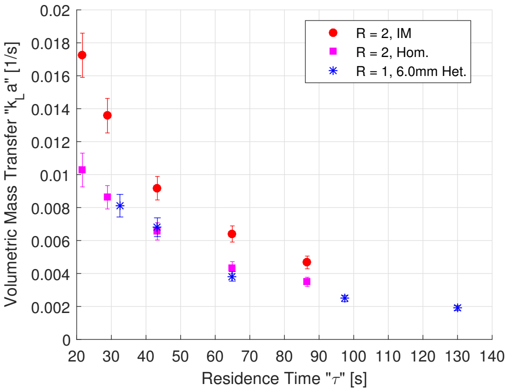

Figure 5.10: Different cases compared to each other for the liquid-liquid extraction. R is the organic to water ratio, IM stands for ideal mixing, p indicates the patterning, thus p = 0 equals the homogeneous capillary and p = 6 the 6.0 mm heterogeneous capillary.

Figure 5.10 shows the ideal mixing (IM) for R = 2, which is the highest volumetric mass transfer which could be achieved, next to the homogeneous capillary for R = 2 and the heterogeneous capillary with 6.0 mm patterning lengths for R = 1. It can be concluded that the amount of organic phase can be reduced by 50 % when heterogeneous patterning of 6.0 mm is added to the capillary in order to get the same volumetric mass transfer.

Conclusion The heterogeneous patterned capillaries showed the expected flow patterns. Phase inversion, adhesion and passing were observed in the capillaries. The extraction efficiency could be improved when the organic to water ratio was lower than 2. The ideal mixing extraction efficiency could be reached by the heterogeneous capillaries only when the amount of water and organic was equal to each other. An accurate critical capillary number for phase inversion or adhesion could not be determined due to the large error margins. The amount of organic can be reduced from R = 2 to 1 by heterogeneous wetted capillary with 6.0 mm patterning length.

Chapter 6

Three Phase Extraction

6.1 Homogeneous hydrophilic wetted capillary

Three phase extraction experiments are performed with two different gas fractions: 0.22 and 0.33. The total flow is equal to the liquid-liquid experiment with organic to water ratio of 2. The water and total flow was set for all experiments. Therefore, the amount of organic decreases with increasing gas fraction. This experiment was initially done by Mandalahalli [7] to investigate the influence of additional gas on the extraction efficiency. The results with the homogeneous hydrophilic capillary are shown in Figure 6.1.

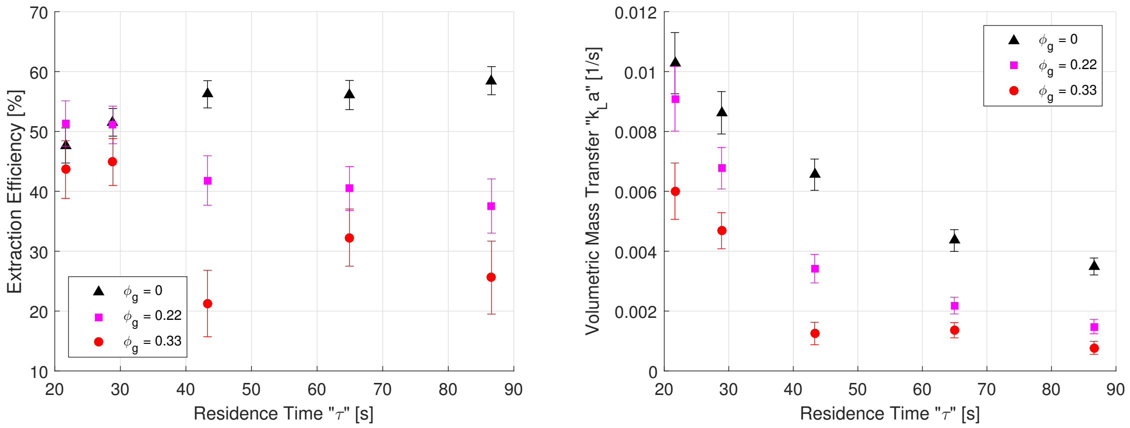

(a) (b)

Figure 6.1: Experimental results in the case of a hydrophilic capillary for different gas fractions and residence times. (a): Extraction efficiency. (b): Volumetric mass transfer coefficient.

Figure 6.1(a) shows the extraction efficiency for increasing gas fraction thus decreasing organic phase. The extraction efficiency slightly improves with increasing residence time when there is no gas present, which was also shown in the previous chapter. The extraction efficiency decreases with increasing gas fraction and residence time. Water is the continuous phase with gas slugs inside the organic slugs (double emulsion, as was shown in Figure 2.3). The gas slug is surrounded with a film layer of organic phase. The film layer saturates really fast and the internal slug circulations are not strong enough to refresh the film layer. It was shown that the extraction efficiency decreases with decreasing amount of organic phase, accounting for the decrease with increasing gas fraction. Figure 6.1(b) shows the volumetric mass transfer coefficient, which also decreases with increasing gas fraction and residence time. The interfacial area is calculated for the lowest gas fraction, $\phi_g = 0.22$ and shown in Figure 6.2, together with the mass transfer coefficient.

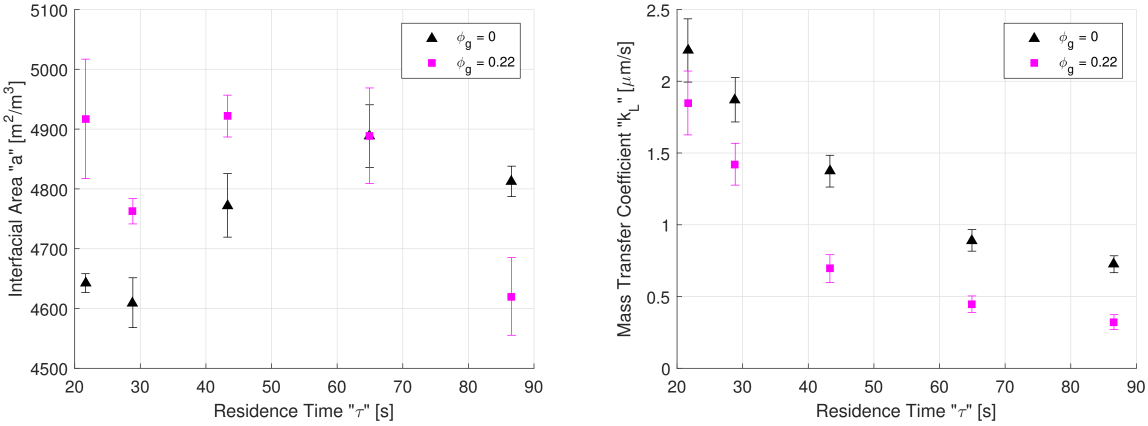

(a) (b)

Figure 6.2: Experimental results in the case of a hydrophilic capillary for different gas fractions and residence times. (a): Interfacial area. (b): Mass transfer coefficient.

The interfacial area increases slightly with increasing gas fraction, except for the highest residence time. The mass transfer coefficient is calculated with the interfacial area and volumetric mass transfer coefficient. It can be seen that the volumetric mass transfer coefficient is slightly lower compared to the liquid-liquid extraction. It can be concluded that the additional gas does not increase the mass transfer for these extraction experiments due to the saturated film layer around the gas slug, which was also concluded by Mandalahalli [7].

6.2 Heterogeneous wetted capillary

6.2.1 Flow patterns

Two different patterning lengths are used for the three phase extraction experiments. For the two phase it was seen that adhesion, phase inversion or passing occurred in the patterned capillary. Only passing was observed for the three phase flow, which can be seen in Figure 6.3.

The first observation made looking at Figure 6.3 is that the organic phase is the continuous phase for the patterned capillaries. Also, the homogeneous capillary looks more like a double emulsion while the heterogeneous capillaries have alternating water and gas slugs. Double emulsion is not possible in the case of patterned capillaries since the hydrophilic water has no affinity with the hydrophobic nitrogen gas. In all cases, there was no sign of water adhesion on the hydrophilic parts of the capillary with heterogeneous wetted capillaries.

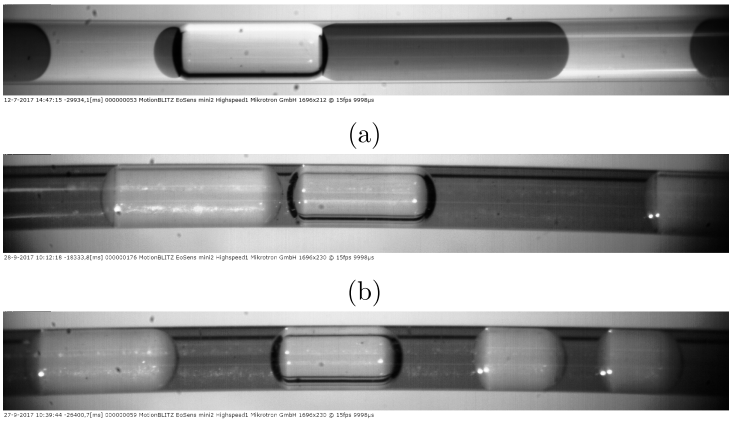

(a)

(b)

(c)

Figure 6.3: Difference in flow patterns for $Q_{\mathrm{wat}} = 40$ µL/min and $\phi_{\mathrm{g}} = 0.22$ in (a) homogeneous, (b) 1.0 mm patterning and (c) 6.0 mm patterned capillary.

The patterning was checked after the experiments, where it became clear that not as much water adhered to the hydrophilic parts of the capillary as directly after hydrophobization. Therefore, it could be that the surface properties were altered chemically by the octanol. An experiment was conducted where the contact angle is measured of four different glass slices (same prodecure as for the other contact angle measurements, see Chapter 4.2). A hydrophilic and hydrophobic glass slice are exposed to 1-octanol with 0.5 wt% Sudan IV for four hours before measuring the contact angle. The glass slices were exposed to octanol for four hours to research the long time effect of octanol on glass since. The results are shown in Table 6.1.

Table 6.1: Contact angle of MilliQ water and 0.5 wt% Sudan IV in 1-octanol on hydrophilic and OTES hydrophobized glass surfaces with and without being in contact with 0.5 wt% Sudan IV in 1-octanol for 4 hours.

Type glass	MilliQ (°)	Sudan IV (°)
Hydrophilic	5.6 ± 1.0	32.4 ± 4.7
Hydrophilic with 1-octanol exposure	22.8 ± 5.7	30.7 ± 3.2
Hydrophobic	74.6 ± 5.5	30.7 ± 4.6
Hydrophobic with 1-octanol exposure	68.1 ± 5.0	30.3 ± 4.6

The contact angle of Sudan IV in 1-octanol remains constant, independent of the type of glass. There even is no difference between the hydrophilic and hydrophobic glass due to the partial hydrophilic and hydrophobic structure of octanol. The water spreads out on hydrophilic glass, but when the hydrophilic glass is exposed to octanol for four hours, the contact angle increases. Therefore, it can be concluded that the octanol alters the hydrophilic surface in such a way that the contact angle of water increases. There is no change in contact angle for the hydrophobic glass.

6.2.2 Extraction results

The extraction experiments were performed for 1.0 and 6.0 mm heterogeneous patterned capillaries. The results are shown in Figure 6.4, sorted for the different gas fractions.

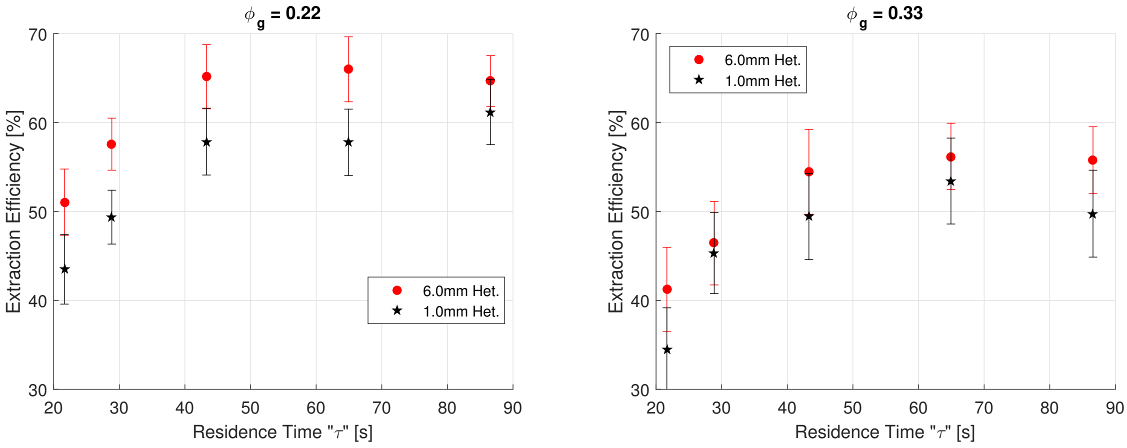

(a) (b)

Figure 6.4: Extraction efficiency for the heterogeneous capillaries with two different patterning lengths: 1.0 and 6.0 mm. (a) $\phi_g = 0.22$ and R = 1.33. (b) $\phi_g = 0.33$ and R = 1.

For both gas fractions there is an increase in extraction efficiency with the patterning. For $\phi_g = 0.33$ there is no difference between the patterning lengths while for $\phi_g = 0.22$ the patterning of 6.0 mm has a bit higher extraction efficiency. However, there was a similar flow pattern observed which should be comparable to the flow pattern in a homogeneous hydrophobic capillary. A decrease in extraction efficiency was observed for the homogeneous capillary due to the saturated organic film layer around the gas slug. Figure 6.3 showed an alternating slug pattern. With an alternating slug pattern there is no saturated film layer which decreases the extraction efficiency. Influence of the alternating slug pattern compared to the double emulsion is investigated by determining the interfacial area in one case, with $\phi_g = 0.22$, R = 1.33 and 1.0 mm patterned heterogeneous capillary. The interfacial area and mass transfers coefficient is shown in Figure 6.5.

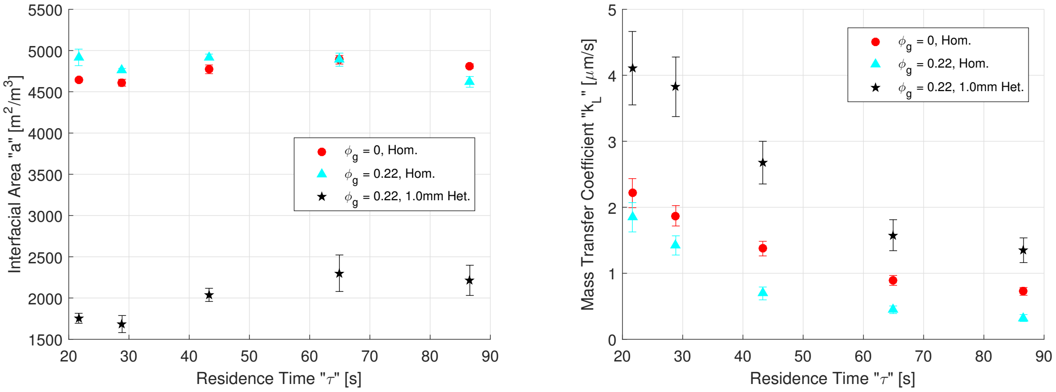

(a) (b)

Figure 6.5: The interfacial area (a) and mass transfer coefficient (b) for a homogeneous hydrophilic capillary with organic to water ratio of 2 ($\phi_g = 0$, R = 2), three phase flow through a homogeneous capillary ($\phi_g = 0.22$, R = 1.33) and lastly with three phase flow in a heterogeneous patterned capillary ($\phi_g = 0.22$, 1.0mm Het).

The interfacial area is between 4500 and 5000 m^2/m^3 for the homogeneous hydrophilic capillaries. The three phase flow with a heterogeneous capillary showed alternating gas liquid slugs instead of a double emulsion, as was seen for the homogeneous capillary. This decreases the interfacial area drastically, as can be seen in Figure 6.5(a). The corresponding mass transfer coefficient was calculated and shown in Figure 6.5(b). An increase in mass transfer coefficient is observed due to the decrease in interfacial area. The mass transfer coefficient is almost doubled, comparing it to the two phase extraction in a homogeneous hydrophilic capillary. The interfacial area for $\phi_g = 0.33$ could not be determined due to the irregular flow pattern. In order to make a fair comparison, the extraction performance and interfacial in a homogeneous hydrophobic should be measured. Also, a more stable flow should be achieved to determine the interfacial area more specifically.

The volumetric mass transfer is calculated for $\phi_g = 0.22$ and $\phi_g = 0.33$ and are shown in Figure 6.6.

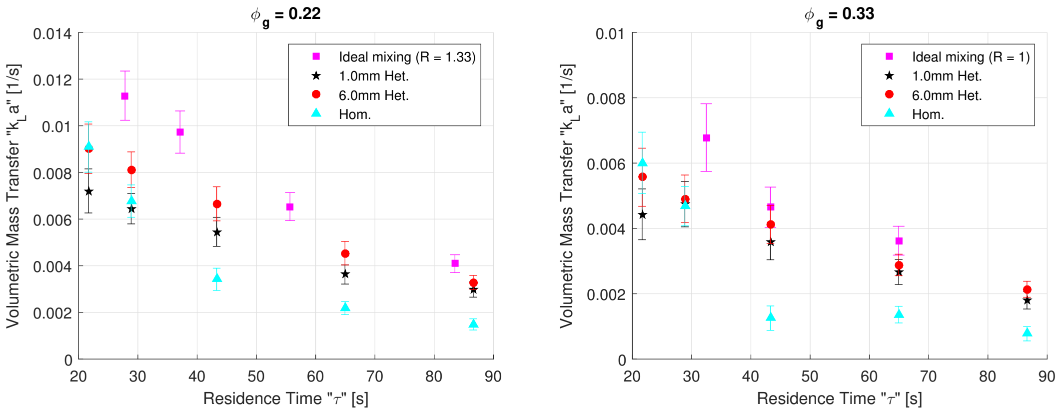

(a) (b)

Figure 6.6: Volumetric mass transfer for the homogeneous and heterogeneous capillaries compared to the ideal mixing case, (a) for $\phi_g = 0.22$ and (b) for $\phi_g = 0.33$.

The mass transfer is enhanced compared to the homogeneous capillaries and even reaches the ideal mixing for $\phi_g = 0.33$ and 6.0 mm patterning length. However, the volumetric mass transfer is in overall higher for the $\phi_g = 0.22$. Figure 6.7 shows how this result correlates to the liquid-liquid extraction with R = 2.

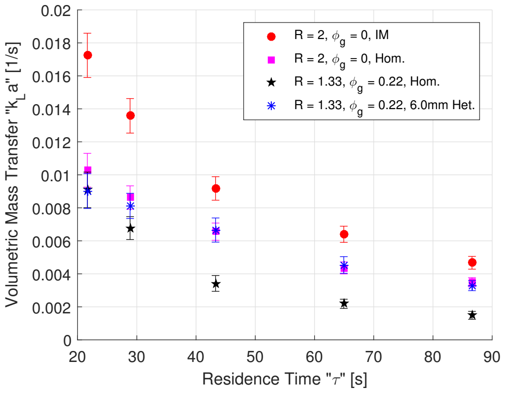

Figure 6.7: Different cases compared to each other for the three phase extraction, where R gives the organic to water ratio, ϕ_g the gas fraction, IM the ideal mixing and p the patterning length of the heterogeneous capillaries, with p = 0 is the homogeneous hydrophilic capillary.

Figure 6.7 shows the volumetric mass transfer for ideal mixing for R = 2, the liquid-liquid extraction for R = 2 and $\phi_g = 0.22$ with and without patterning. The volumetric mass transfer decreases by introducing the gas fraction and reducing the amount of organic phase. This decrease can be overcome by the addition of heterogeneous surface wettability with 6.0 mm patterning length. However, the same could be achieved with the two phase system for R = 1 while the three phase has R = 1.33 and $\phi_g = 0.22$.

Conclusion The extraction efficiency could successfully be enhanced with the heterogeneous patterned capillaries. The flow patterned switched from double emulsion to alternating slugs with the heterogeneous capillaries, but there was no phase inversion or adhesion visible. The increase in extraction efficiency is due to the change in flow pattern, which is not influenced by a saturated film layer. The mass transfer can be enhanced with $\phi_{\mathrm{g}} = 0.22$, R = 1.33 and 6 mm heterogeneous patterning up to the same mass transfer of R = 2 for a homogeneous hydrophilic capillary, thus the organic to water ratio could be decreased from 2 to 1.33. It should be investigated if this result is also possible with a homogeneous hydrophobic capillary.

Chapter 7

Conclusion and Recommendations

The goal of this research was to study the effect of heterogeneous surface wettability on mixing patterns and the resulting extraction in circular capillaries. The goal is achieved by studying the liquid-liquid and gas-liquid-liquid extraction in homogeneous hydrophilic capillaries before introducing the heterogeneous wetted capillary. Additionally, the influence of phase interactions, hydrodynamics, cleaning, mixing and separation were studied. The chosen model system was 1 wt% acetic acid in water with 0.5 wt% Sudan IV in 1-octanol. The Sudan IV is added to increase visibility between the phases. The addition of acetic acid to water and Sudan IV to 1-octanol did not change the interfacial and surface tension significantly for the system. Solid-liquid interactions are highly dependent on the solid properties. From the contact angle analysis, it could be determined that full phase inversion is possible with the used model system. The two liquids are mixed in a T-junction where the octanol is squeezed in the water phase, creating a slug flow in the capillary. The capillary was beforehand thoroughly cleaned with concentrated potassium hydroxide and nitric acid. A settler is used at the end of the capillary to collect both liquids and separate them based on gravity. The concentration of acetic acid is determined in the water phase by the conductivity measurements.

The two phase extraction was measured for different organic to water ratios, ranging from 2 to 1. For the homogeneous hydrophilic capillary, the extraction efficiency, volumetric mass transfer and interfacial area decreased with decreasing organic to water ratio. The maximum extraction efficiency of ±60% was obtained for R = 2 and τ = 90s. The mass transfer coefficient decreased with increasing residence time, proportional to the superficial velocity of the liquids. The heterogeneous patterned capillaries showed different flow patterns. Passing, phase inversion and adhesion were observed for the pattering length of 6.0 mm, while only passing and adhesion were shown for 1.0 mm patterning length. The critical Capillary number was calculated for phase inversion and adhesion, with a fitting parameter of $k_{\text{phase inversion}} = 1.66 \pm 0.64$ and $k_{\text{adhesion}} = 2.09 \pm 0.88$. The fitting parameter for phase inversion and adhesion overlap, therefore it is not a good estimation of the critical Capillary number. The impact of heterogeneous patterned capillaries increased with decreasing organic to water ratio. For the organic to water ratio of 2 there was no increase in volumetric mass transfer whilst the ideal mixing could be achieved with the ratio of 1. Overall, the organic to water ratio could be halved (from R = 2 to R = 1) by introducing the heterogeneous wetted capillaries with a patterning length of 6.0 mm.

The three phase extraction was measured with increasing amount of gas while keeping the total flow rate constant, thus decreasing the amount of organic. For the homogeneous hydrophilic capillary it was observed that the extraction efficiency and volumetric mass transfer decrease with increasing amount of gas. A double emulsion flow pattern was shown which has the disadvantage of a saturated film layer around the gas slug. Therefore, the additional gas could not enhance the extraction. Heterogeneous patterning was successfully added to overcome this mass transfer limitation. However, there was no phase inversion or even adhesion observed with the patterning. The capillary appeared completely hydrophobic with alternating gas-water slugs in the organic continuous phase. The contact angle was measured on a glass surface which was exposed to octanol for four hours, where it was seen that octanol caused an increase in contact angle for water on the hydrophilic surface. The inversion of continuous phase did enhance the mass transfer due to the missing film layer around the gas slug. Overall, the volumetric mass transfer of R = 2 for the hydrophilic capillary could be reached with $\phi_{\mathrm{g}} = 0.22$ in a heterogeneous patterned capillary with 6.0 mm patterning.

In conclusion, the volumetric mass transfer coefficient of the organic to water ratio of 2 with the homogeneous hydrophilic capillary could be reached by the addition of 6.0 mm heterogeneous wetted surface with two and three phase extraction. The amount of organic could be halved with the patterning length of 6.0 mm for two phase extraction. For three phase extraction the same result could be reached for the same patterning length with $\phi_{\mathrm{g}} = 0.22$. Overall, the heterogeneous wetted surface is a promising technique for two phase extraction. For three phase it is a devious method, since a lot of effort need to be put in without achieving the same decrease in organic to water ratio compared to the liquid-liquid extraction.

7.1 Recommendations

Several recommendations can be made for further research.

1. The hydrophobization method could be improved with different hydrophobization agents. The main goal would be to make the method as easy and robust as possible. In the research it was shown that OTES is not as hydrophobic as FDTS, which influenced the results. With an improved hydrophobization technique, phase inversion and adhesion might also be possible for the three phase extraction thus enhancing the mass transfer. Additionally, extractions experiments should also be conducted in a completely hydrophobic capillary. The three phase extraction already showed an increase in performance, but the effect is unknown for the two phase extraction.

2. The ideal mixing efficiency is not reached for the higher organic to water ratios. Therefore, more rigorous mixing could be induced to reach this efficiency. This could be done with for example combining a micro mixer with the capillary or decreasing the patterning lengths even more (0.1 mm) to see if there is a limit.

3. The physical insights could be enhance by a COMSOL model. It was already shown that modelling in COMSOL is possible, but a numerical validation was left out. The numerical model could increase the insights in mixing patterns. Ideally, the numerical model predicts the extraction performance which makes optimizing the patterning easier.

4. The organic to water ratio was decreased with the heterogeneous patterning. More systems could be used to investigate if it works for more extractions. Especially systems with an very expensive solvent should be investigated.

Chapter 8

Bibliography

[1] J. D. Seader, Ernest J. Henley, and D. Keith Roper. *Separation Process Principles: Chemical and Biochemical Operations*. JOHN WILEY & SONS INC, 2010. ISBN 0470481838.

[2] Cong Xu and Tingliang Xie. Review of microfluidic liquid-liquid extractors. *Industrial & Engineering Chemistry Research*, 56(27):7593–7622, 2017. doi: 10.1021/acs.iecr.7b01712.

[3] N. Assmann, A. Ładosz, and P. Rudolf von Rohr. Continuous micro liquid-liquid extraction. *Chemical Engineering & Technology*, 36(6):921–936, apr 2013. doi: 10.1002/ceat.201200557.

[4] Kai Wang and Guangsheng Luo. Microflow extraction: A review of recent development. *Chemical Engineering Science*, oct 2016. doi: 10.1016/j.ces.2016.10.025.

[5] Kai Wang, Kang Qin, Tao Wang, and Guangsheng Luo. Ultra-thin liquid film extraction based on a gas–liquid–liquid double emulsion in a microchannel device. *RSC Adv.*, 5(9): 6470–6474, 2015. doi: 10.1039/c4ra14489a.

[6] Nam-Trung Nguyen and Zhigang Wu. Micromixers - a review. *Journal of micromechanics and microengineering*, 15(2):R1, 2004.

[7] Manas Manohar Mandalahalli. Intensification of extraction using gas-liquid-liquid system. Master's thesis, University of Twente, 2015.

[8] Qiang Meng, Yali Zhang, Jiang Li, Rob G. H. Lammertink, Haosheng Chen, and Peichun Amy Tsai. Altering emulsion stability with heterogeneous surface wettability. *Scientific Reports*, 6:26953, jun 2016. doi: 10.1038/srep26953.

[9] Ian Gentle Geoffrey Barnes. *Interfacial Science: An Introduction*. Oxford University Press, 2011. ISBN 019957118X.

[10] Yuanhai Su, Yuchao Zhao, Guangwen Chen, and Quan Yuan. Liquid-liquid two-phase flow and mass transfer characteristics in packed microchannels. *Chemical Engineering Science*, 65(13):3947–3956, 2010.

[11] Milan Sovilj. Hydrodynamics of gas-agitated liquid-liquid extraction columns. *Acta periodica technologica*, 43(43):199–216, 2012. doi: 10.2298/apt1243199s.

[12] J. Tan, Z.D. Liu, Y.C. Lu, J.H. Xu, and G.S. Luo. Process intensification of H_2O_2 extraction using gas–liquid–liquid microdispersion system. *Separation and Purification Technology*, 80 (2):225–234, jul 2011. doi: 10.1016/j.seppur.2011.04.030.

[13] Arata Aota, Masaki Nonaka, Akihide Hibara, and Takehiko Kitamori. Countercurrent laminar microflow for highly efficient solvent extraction. *Angewandte Chemie*, 119(6): 896–898, 2007.

[14] Javier Atencia and David J Beebe. Controlled microfluidic interfaces. *Nature*, 437(7059): 648, 2005.

[15] Muireann OâĂŹLoughlin, Craig Priest, Mihail N Popescu, and John Ralston. Patterning of wettability for controlling capillary-driven flow in closed channels. *Journal of colloid and interface science*, 402:259–266, 2013.

[16] Yuchao Zhao, Yuanhai Su, Guangwen Chen, and Quan Yuan. Effect of surface properties on the flow characteristics and mass transfer performance in microchannels. *Chemical Engineering Science*, 65(5):1563–1570, 2010.

[17] Robert H. Perry and Don W. Green. *Perry's Chemical Engineers' Handbook*. McGraw-Hill Professional, 1997. ISBN 0-07-049841-5.

[18] Oliver Brand, Gary K. Fedder, Christofer Hierold, Jan G. Korvink, and Osamu Tabata. *Micro Process Engineering*. Wiley VCH Verlag GmbH, 2006. ISBN 3527312463.

[19] Ken-Ichiro Sotowa. Fluid behavior and mass transport characteristics of gas-liquid and liquid-liquid flows in microchannels. *Journal of Chemical Engineering of Japan*, 47(3): 213–224, 2014. doi: 10.1252/jcej.13we141.

[20] Léon Peter Bernard Marie Janssen and Marinus Maria Cornelis Gerardus Warmoeskerken. *Transport phenomena data companion*. VSSD, 3rd edition, 2006. ISBN 90-71301-59-1.

[21] Norbert Kockmann. *Transport phenomena in micro process engineering*. Springer Science & Business Media, 2007. ISBN 978-3-540-74618-8.

[22] Lukas Hohmann, Safa Kutup Kurt, Sebastian Soboll, and Norbert Kockmann. Separation units and equipment for lab-scale process development. *Journal of Flow Chemistry*, 6(3): 181–190, 2016.

[23] Marc Mac Giolla Eain, Vanessa Egan, and Jeff Punch. Film thickness measurements in liquid–liquid slug flow regimes. *International Journal of Heat and Fluid Flow*, 44:515–523, 2013.

[24] Aras Ghaini, Axel Mescher, and David W Agar. Hydrodynamic studies of liquid–liquid slug flows in circular microchannels. *Chemical engineering science*, 66(6):1168–1178, 2011.

[25] MN Kashid, I Gerlach, S Goetz, J Franzke, JF Acker, F Platte, DW Agar, and S1 Turek. Internal circulation within the liquid slugs of a liquid- liquid slug-flow capillary microreactor. *Industrial & engineering chemistry research*, 44(14):5003–5010, 2005.

[26] Haosheng Chen, Enkai Dong, Jiang Li, and Howard A Stone. Adhesion of moving droplets in microchannels. *Applied Physics Letters*, 103(13):131605, 2013.

[27] Xianmin Xu and Xiaoping Wang. Analysis of wetting and contact angle hysteresis on chemically patterned surfaces. *SIAM journal on applied mathematics*, 71(5):1753–1779, 2011.

[28] Madhvanand N. Kashid, Albert Renken, and Lioubov Kiwi-Minsker. Gas–liquid and liquid–liquid mass transfer in microstructured reactors. *Chemical Engineering Science*, 66 (17):3876–3897, sep 2011. doi: 10.1016/j.ces.2011.05.015.

[29] ImageJ. URL `http://imagej.net`.

[30] Engineering Toolbox. URL `http://www.engineeringtoolbox.com/gases-absolute-dynamic-viscosity-d_1888.html`.

[31] Dataphysics Instruments GmbH. Pendant drop method - optical determination of the surface/interfacial tension. URL `http://www.dataphysics.de/2/start/understanding-interfaces/drop-shape-analysis/pendant-drop-method/`.

[32] Joseph D Berry, Michael J Neeson, Raymond R Dagastine, Derek YC Chan, and Rico F Tabor. Measurement of surface and interfacial tension using pendant drop tensiometry. *Journal of colloid and interface science*, 454:226–237, 2015.

[33] CJ Van Oss, RJ Good, and MK Chaudhury. Additive and nonadditive surface tension components and the interpretation of contact angles. *Langmuir*, 4(4):884–891, 1988.

[34] Ju Chin Chu, Clifford C Taylor, and Donald J Levy. Liquid-liquid extraction correlation of htu with interfacial tension. *Industrial & Engineering Chemistry*, 42(6):1157–1163, 1950.

[35] Charles L Bowman. Quantifying the cleanliness of glass capillaries. *Cell biochemistry and biophysics*, 29(3):203–223, 1998.

[36] Dongying Qian and Adeniyi Lawal. Numerical study on gas and liquid slugs for taylor flow in a t-junction microchannel. *Chemical Engineering Science*, 61(23):7609–7625, 2006.

[37] Piotr Garstecki, Michael J Fuerstman, Howard A Stone, and George M Whitesides. Formation of droplets and bubbles in a microfluidic t-junctionâĂŤscaling and mechanism of break-up. *Lab on a Chip*, 6(3):437–446, 2006.

[38] Madhvanand N Kashid and David W Agar. Hydrodynamics of liquid–liquid slug flow capillary microreactor: flow regimes, slug size and pressure drop. *Chemical Engineering Journal*, 131(1):1–13, 2007.

[39] Jovan Jovanović, Wenya Zhou, Evgeny V Rebrov, TA Nijhuis, Volker Hessel, and Jaap C Schouten. Liquid–liquid slug flow: hydrodynamics and pressure drop. *Chemical Engineering Science*, 66(1):42–54, 2011.

[40] Agnieszka Ładosz, Eugen Rigger, and Philipp Rudolf von Rohr. Pressure drop of three-phase liquid–liquid–gas slug flow in round microchannels. *Microfluidics and Nanofluidics*, 20(3): 49, 2016.

[41] Nelly Hobeika, Patrick Bouriat, Abdelhafid Touil, Daniel Broseta, Ross Brown, and Jean Dubessy. Help from a hindrance: using astigmatism in round capillaries to study contact angles and wetting layers. *Langmuir*, 2017.

Appendix A

Project Description

This is the original description of the master assignment

The enhancement of mass transfer/extraction efficiency of liquid-liquid (LL) extraction systems using an inert gas phase (GLL) is an interesting phenomena with applicability to a wide number of systems. More recently, work has been done to measure the extraction performance and mechanism by studying the process at smaller length scales in capillaries (mm scale) by performing extractions and measuring the resulting flow patterns by visualization (high-speed camera). At these scales, the interfacial forces cannot be neglected and play an important role in phase stability and the nature of flow through the system; parallel-flows or two- and three-phase slug flows may arise, which have important implications for the mass transfer efficiency in these types of systems. The mechanism behind this enhancement is presently under investigation, requiring detailed measurements at varying flow conditions in order to determine the gas effect on various process parameters. These include interfacial area between liquid phases and the stability of flow regimes for example.

The purpose of the proposed assignment is to investigate the influence of patterned wettability gradients in a capillary on the two- and three-phase flows (LL and GLL) and liquid-liquid extraction in these systems. Switching between hydrophilic and hydrophobic domains in a periodic fashion can lead to phase inversions/mixing patterns which may greatly enhance mass transfer. This will be accomplished through image/video capture using a high-speed camera, with subsequent flow patterns characterized using image analysis. Study of these flow patterns is then highly relevant for quantifying what possible enhancements can be realized through the use of such patterned-capillaries. Corresponding liquid-liquid extractions will be investigated using an established model system (acetic acid-water-octanol) initially, with an emphasis on determining the role of gas and wettability patterning on the resulting extraction efficiencies vs. a two-phase flow system.

Appendix B

Interfacial Area Calculations

The interfacial area is determined by measuring different lengths from the obtained images made with the high speed camera. This appendix gives all the used equations in order to calculate the specific area. There is no error analysis performed in this case, since the interfacial area of three different slugs is calculated for each experiment. The standard deviation between these slugs will be used as error, since it is a larger error compared to the possible error from measuring.

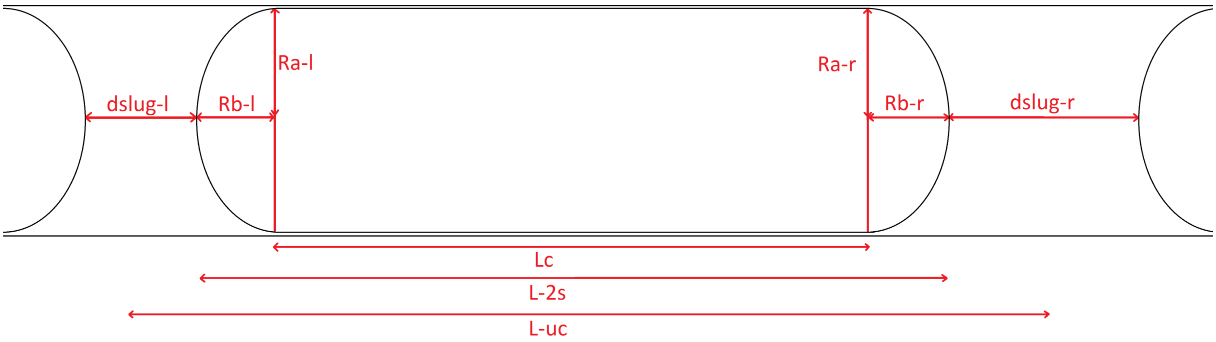

Figure B.1: Schematic of the interfacial area.

The slug is divided in three parts: front cap, cylindrical middle and end cap, see Figure B.1. Both caps are considered to be ellipsoidal, a prolate or oblate spheroid to be more precise. The two radii of the caps are measured, together with the total slug length. The middle part length is calculated from the total slug length and horizontal radii. The film layer around the middle part is calculated with the following equation:

$$\frac{h}{r} = 0.35(Ca)^{0.354}(We)^{0.097} \tag{B.1}$$

For the caps one has to take into account the refractive index of the glass, which causes the vertical radii to look longer then they are [41]. The real radius (R_i) is calculated from the refractive index (n), apparent radius (R_a) and the outer radius (R_o), with the following equation:

$$R_i = \frac{R_a}{n \cdot \sqrt{1 - \frac{R_a^2}{R_o^2}} \cdot \sqrt{1 - \frac{R_a^2}{n^2 R_o^2} + \frac{R_a^2}{R_o^2}}} \tag{B.2}$$

As said before, the caps can be a prolate or oblate spheroid. For a prolate spheroid the vertical radius (R_i) is larger than the horizontal (R_b), for oblate the other way around. Both spheroids have a different equation to calculate the interfacial area. For the prolate ellipsoid is it the following equation for halve an ellipsoid:

$$a_{\text{prolate}} = \pi R_b^2 \cdot \left(1 + \frac{R_i}{R_b\sqrt{1-\frac{R_b^2}{R_i^2}}} \cdot \sin^{-1}\left(\sqrt{1-\frac{R_b^2}{R_i^2}}\right)\right) \tag{B.3}$$

And for an oblate spheroid:

$$a_{\text{oblate}} = \pi R_b^2 \cdot \left(1 + \frac{1-\sqrt{1-\frac{R_i^2}{R_b^2}}}{\sqrt{1-\frac{R_i^2}{R_b^2}}} \cdot \tanh^{-1}\left(\sqrt{1-\frac{R_i^2}{R_b^2}}\right)\right) \tag{B.4}$$

The total area is calculated by the summation of the interfacial area of both caps and the film layer. The volume of the unit cell is calculated with the length of the unit cell and channel radius:

$$V_{\text{unit cell}} = \pi L_{\text{unit cell}} r_{\text{channel}}^2 \tag{B.5}$$

The length of the unit cell is the length of the slug plus halve the lengths to the next slug and previous slug. The final interfacial area is calculated by dividing the calculated area by the volume of the unit cell.

Appendix C

Error Analysis Extraction Performance

An error analysis can be applied on the calculations for the specific area and mass transfer coefficient. First, it is explained how the error analysis is executed. Secondly, the error analysis for the mass transfer coefficient is shown and finally, the error in the specific area is given.

C.1 Method

Two separate errors can be distinguished: the possible and statistical error. The possible error is focussed on the absolute values of all measured point. The statistical error gives te 95% reliability interval, therefor it decreases with increasing amount of experiments. The possible error increases with the increase in amount of experiments, since it relies on the absolute values. The statistical error is used in this work.

The statistical error is calculated as following for adding ($z = x + y$) and substracting ($z = x - y$).

$$s_z^2 = s_x^2 + s_y^2 \tag{C.1}$$

All other statistical errors can be derived according to the following equation (where $z = z(x, y)$).

$$s_z^2 = \left(\frac{\partial z}{\partial x}\right)^2 s_x^2 + \left(\frac{\partial z}{\partial y}\right)^2 s_y^2 \tag{C.2}$$

With the equations shown above, all errors could be determined. Most errors are calculated, some are measured, some are fabrication errors and some are estimated.

C.2 Mass Transfer Performance

A mass balance over the water phase is made in order to calculate the extraction efficiency and mass transfer coefficient. These were defined as following:

$$E = \frac{w_{aq,in} - w_{aq,out}}{w_{aq,in} - w_{aq,eq}} \tag{C.3}$$

$$k_L a = \frac{1}{\tau\left(\frac{1}{K\epsilon_{aq}} + \frac{1}{\epsilon_{org}}\right)} \log\left(\frac{w_{aq,in} - w_{aq,eq}}{w_{aq,out} - w_{aq,eq}}\right) \tag{C.4}$$

The errors which are estimated are shown below in the table. All the other errors are calculated from these errors.

Error	Origin	Value
s_Q	Estimated	1 %
s_m	Analytical balance	10^{-4} g
s_m	Balance	0.1 g
$s_{d_{channel}}$	Fabrication	0.05 mm
$s_{L_{channel}}$	Estimated	0.05 mm
s_ρ	Estimated	2 kg/m^3
s_{K_d}	Estimated	0.005
s_κ	Estimated	0.5 %

The weight fraction at the start of the capillary is known (set at 1 wt%). The equilibrium concentration is calculated with the begin concentration, density and phase holdup. The concentration at the outlet is calculated via a calibration sequence of the conductivity versus concentration.

$$w_{aq,out,dil} = \frac{\kappa - a}{b} \tag{C.5a}$$

$$s^2_{w_{aq,out,dil}} = \frac{s^2_\kappa}{b^2} \tag{C.5b}$$

where κ is the conductivity and a and b are fitted parameters.

The outlet concentration is then calculated by

$$w_{aq,out} = w_{aq,out,dil}\left(1 + \frac{m_{diluted}}{m_{original}}\right) \tag{C.6a}$$

$$s^2_{w_{aq,out}} = \left(1 + \frac{m_{dil}}{m_{orig}}\right)^2 s^2_{w_{aq,out,dil}} + \left(\frac{w_{aq,out,dil}}{m_{orig}}\right)^2 \left(s^2_{m_{dil}} + \left(\frac{m_{dil}}{m_{orig}}\right)^2 s^2_{m_{orig}}\right) \tag{C.6b}$$

And the equilibrium concentration

$$w_{aq,eq} = \frac{w_{aq,in}}{1 + K_d \frac{\rho_{org}}{\rho_{aq}}\frac{\epsilon_{org}}{\epsilon_{aq}}} \tag{C.7a}$$

$$\begin{aligned} s^2_{w_{aq,eq}} = {} & \left(\frac{1}{1 + K_d \frac{\rho_{org}}{\rho_{aq}}\frac{\epsilon_{org}}{\epsilon_{aq}}}\right)^2 s^2_{w_{aq,in}} + \left(\frac{K_d \rho_{org}\epsilon_{org}}{(K_d\rho_{org}\epsilon_{org} + \rho_{aq}\epsilon_{aq})^2}\right)^2 (\epsilon_{aq} s^2_{\rho_{aq}} + \rho_{aq} s^2_{\epsilon_{aq}}) + \\ & \frac{\left(\frac{\rho_{org}}{\rho_{aq}}\frac{\epsilon_{org}}{\epsilon_{aq}}\right)^2 s^2_{K_d} + \left(\frac{K_d}{\rho_{aq}}\frac{\epsilon_{org}}{\epsilon_{aq}}\right)^2 s^2_{\rho_{org}} + \left(\frac{\rho_{org}}{\rho_{aq}}\frac{K_d}{\epsilon_{aq}}\right)^2 s^2_{\epsilon_{org}}}{\left(1 + K_d \frac{\rho_{org}}{\rho_{aq}}\frac{\epsilon_{org}}{\epsilon_{aq}}\right)^4} \end{aligned} \tag{C.7b}$$

The extraction efficiency can be calculated with the weight fractions of the inlet, outlet and equilibrium.

$$E = \frac{w_{aq,in} - w_{aq,out}}{w_{aq,in} - w_{aq,eq}} \tag{C.8a}$$

$$s_E^2 = \frac{\left(w_{aq,out} - w_{aq,eq}\right)^2 s_{w_{aq,in}}^2 + \left(w_{aq,in} - w_{aq,out}\right)^2 s_{w_{aq,eq}}^2}{\left(w_{aq,in} - w_{aq,eq}\right)^4} + \frac{s_{w_{out}}^2}{\left(w_{aq,in} - w_{aq,eq}\right)^2} \tag{C.8b}$$

For the mass transfer coefficient a constant or pure inlet concentration the following equations are applicable.

$$k_La = \frac{1}{\tau}\log\left(\frac{w_{aq,in} - w_{aq,eq}}{w_{aq,out} - w_{aq,eq}}\right) \tag{C.9a}$$

$$\begin{split} s_{k_La}^2 = \left(\frac{1}{\tau^2}\log\left(\frac{w_{aq,in} - w_{aq,eq}}{w_{aq,out} - w_{aq,eq}}\right)\right)^2 s_\tau^2 + \frac{s_{w_{aq,out}}^2}{\tau\left(w_{aq,eq} - w_{aq,out}\right)} + \\ \left(\frac{1}{\tau}\frac{w_{aq,out} - w_{aq,in}}{\left(w_{aq,in} - w_{aq,eq}\right)\left(w_{aq,out} - w_{aq,eq}\right)}\right)^2 s_{w_{aq,eq}}^2 \end{split} \tag{C.9b}$$

The partition coefficient is needed for the volumetric mass transfer coefficient, which is defined as following:

$$K = \left(\frac{\rho_{aq}}{\rho_{org}}\right)\frac{1}{K_d} \tag{C.10a}$$

$$s_K^2 = \frac{1}{\left(K_d\rho_{org}\right)^2}\left(s_{\rho_{aq}}^2 + \left(\frac{\rho_{aq}}{\rho_{org}}\right)^2 s_{\rho_{org}}^2 + \left(\frac{\rho_{aq}}{K_d}\right)^2 s_{K_d}^2\right) \tag{C.10b}$$

So for the mass transfer coefficient:

$$k_La = \frac{1}{\tau\left(\frac{1}{K\epsilon_{aq}} + \frac{1}{\epsilon_{org}}\right)}\log\left(\frac{w_{aq,in} - w_{aq,eq}}{w_{aq,out} - w_{aq,eq}}\right) \tag{C.11a}$$

$$\begin{split} s_{k_La}^2 = \left(\frac{\log\left(\frac{w_{aq,in} - w_{aq,eq}}{w_{aq,out} - w_{aq,eq}}\right)}{\tau\left(K\epsilon_{aq} + \epsilon_{org}\right)^2}\right)^2 \left(\epsilon_{aq}^2\epsilon_{org}^4 s_K^2 + K^2\epsilon_{org}^4 s_{\epsilon_{aq}}^2 + K^4\epsilon_{aq}^4 s_{\epsilon_{org}}^2\right) + \left(\frac{1}{\tau\left(\frac{1}{K\epsilon_{aq}} + \frac{1}{\epsilon_{org}}\right)}\right)^2 * \\ \left(\left(\frac{1}{\tau}\log\left(\frac{w_{aq,in} - w_{aq,eq}}{w_{aq,out} - w_{aq,eq}}\right)\right)^2 s_\tau^2 + \left(\frac{w_{aq,out} - w_{aq,in}}{\left(w_{aq,in} - w_{aq,eq}\right)\left(w_{aq,out} - w_{aq,eq}\right)}\right)^2 s_{w_{aq,eq}}^2 + \frac{s_{w_{aq,out}}^2}{\left(w_{aq,eq} - w_{aq,out}\right)^2}\right) \end{split} \tag{C.11b}$$

Appendix D

Material List Extraction Experiments

This appendix shows the different materials and chemicals used for the extraction performance experiments.

Chemicals:

- Acetic acid: 98% glacial from Sigma-Aldrich
- Sudan IV: Dye content, $\geq$ 80% from Sigma-Aldrich
- 1-octanol: Anhydrous, $\geq$ 99% from Sigma-Aldrich
- Ethanol (for cleaning): Analytical standard from Sigma-Aldrich
- Acetone (for cleaning): For HPLC, $\geq$ 99.9% from Sigma-Aldrich

Materials list for the two phase experiments.

Quantity	Material
1	Picoplus syringe pump
1	NewEra-1000 syringe pump
2	10 mL Terumo syringes with luer lock
5	Two-Piece Fingertight Fittings with ferrules (F-300x) from Inacom
1	PEEK Tee-part (P-728) from Inacom with 1.25 mm thru-hole
-	Hilgenberg borosilicate capillaries, 150mm length / 1.5mm OD / 0.225mm wall thickness
1	Homemade settler
1	Syringe needle
1/EE	2mL BD syringe
1/EE	centrifugal tube
1	Analytical balance
1	Conductivity meter, WTW 3210
1	High speed camera with lens, Motion BLITZ EoSens
1	lamp
-	Spartan 30/0.2 RC Filter units from GE healthcare
-	1/16” tubing

Additional material list for the three phase experiments.

Quantity	Material
1	PEEK Cross (P-730) from Inacom with 1.25 mm thru-hole
1	N_2 dryer
1	Pressure regulator from Linde, 0.5-5 bar outgoing pressure
1	Mass flow controller, 1 mln/min N_2, 10 bar / 3 bar from Bronckhorst

Appendix E

Additional information Methods and Materials

Calibration curve

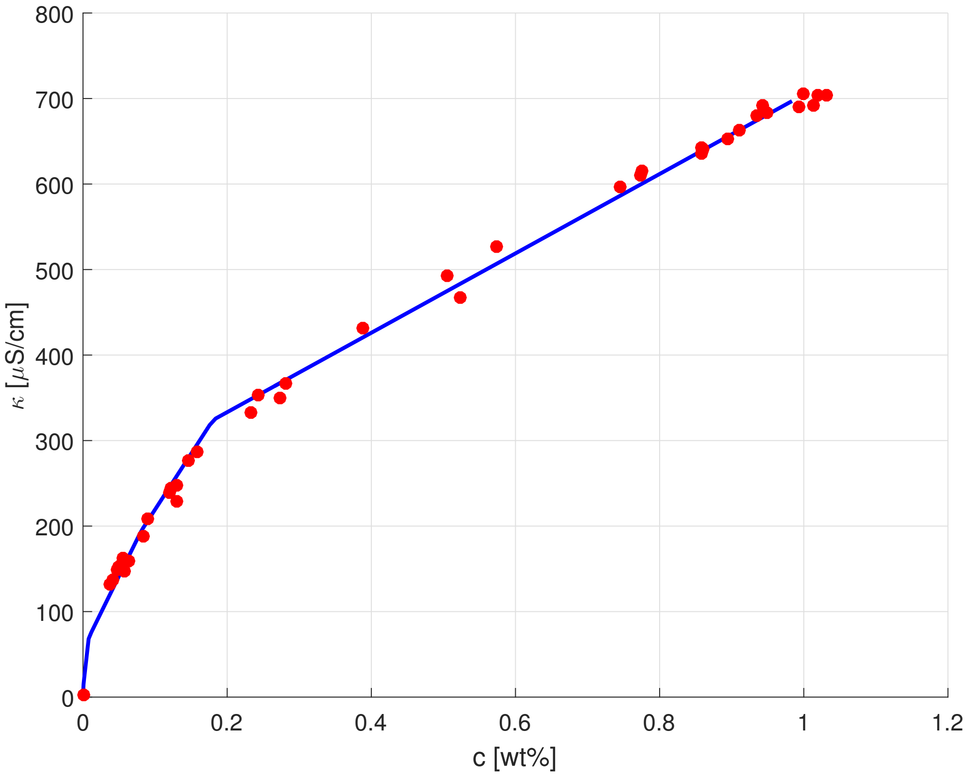

Figure E.1: Concentration of acetic acid versus the electrical conductivity.

Experiments

Table E.1: Liquid-liquid experiments which are performed. The flows (Q) are in μL/min and residence time (τ) in seconds.

		R = 2		R = 1.67		R = 1.33		R = 1	
Q_{wat}	t [min]	Q_{org}	τ	Q_{org}	τ	Q_{org}	τ	Q_{org}	τ
30	50	60	86.6	50	97.4	40	111.3	30	129.9
40	38	80	64.9	67	73.1	53	83.5	40	97.4
60	25	120	43.3	100	48.7	80	55.7	60	64.9
90	17	180	28.9	150	32.5	120	37.1	90	43.3
120	13	240	21.6	200	24.4	160	27.8	120	32.5

Table E.2: Gas-liquid-liquid experiments which are performed. The flows (Q) are in μL/min and residence time (τ) in seconds.

			$\phi_g = 0$		$\phi_g = 0.22$		$\phi_g = 0.33$	
Q_{wat}	τ	t [min]	Q_{org}	Q_{gas}	Q_{org}	Q_{gas}	Q_{org}	Q_{gas}
30	86.6	50	60	0	40	20	30	30
40	64.9	38	80	0	53	26.7	40	40
60	43.3	25	120	0	80	40	60	60
90	28.9	17	180	0	120	60	90	90
120	21.6	13	240	0	160	80	120	120

Appendix F

Additional Information Two Phase Extraction

Additional graphs for the two phase extraction performance.

Homogeneous Wetted Capillary

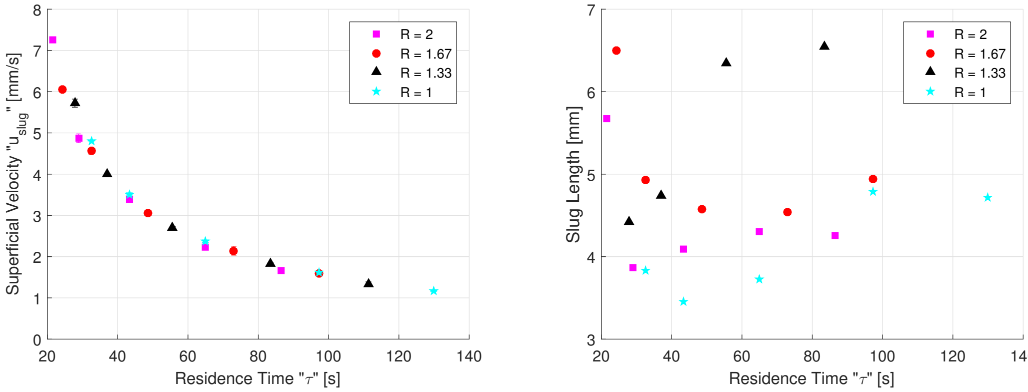

(a)

(b)

Figure F.1: Homogeneous wetted capillary, with the residence time versus the slug velocity and length.

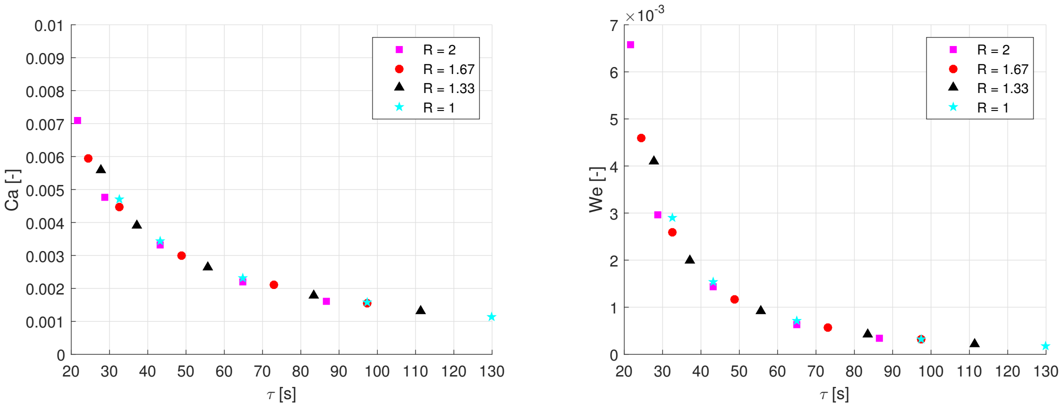

(a) (b)

Figure F.2: The Capillary and Weber number for different residence times and ratios.

Heterogeneous Wetted Capillary

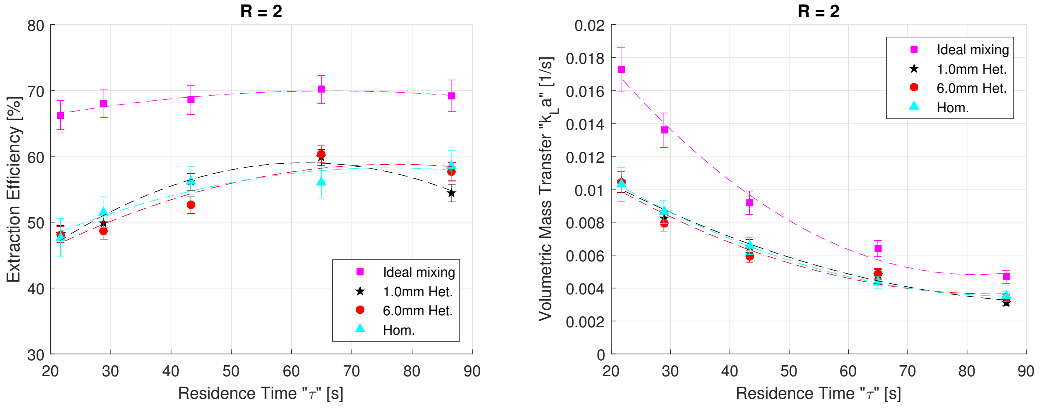

(a) (b)

Figure F.3: The extraction efficiency and volumetric mass transfer coefficient for the organic to water ratio of 2.

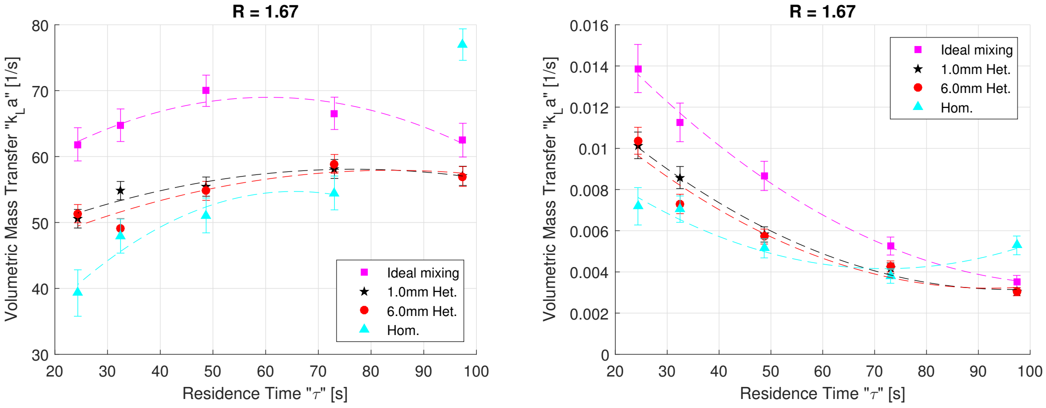

(a) (b)

Figure F.4: The extraction efficiency and volumetric mass transfer coefficient for the organic to water ratio of 1.67.

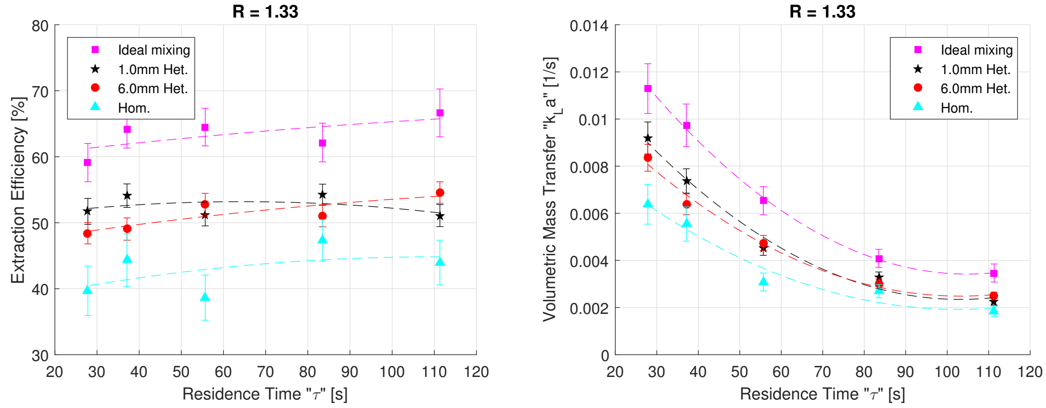

(a) (b)

Figure F.5: The extraction efficiency and volumetric mass transfer coefficient for the organic to water ratio of 1.33.

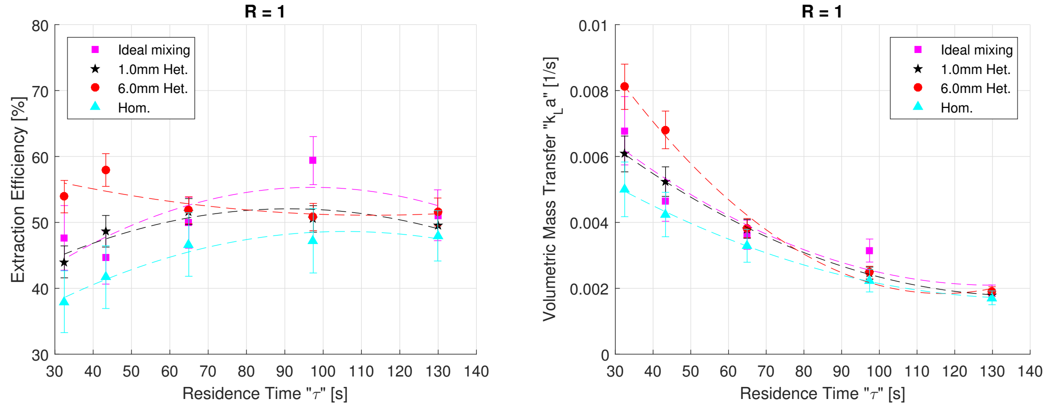

(a) (b)

Figure F.6: The extraction efficiency and volumetric mass transfer coefficient for the organic to water ratio of 1.

Appendix G

Additional Information Three Phase Extraction

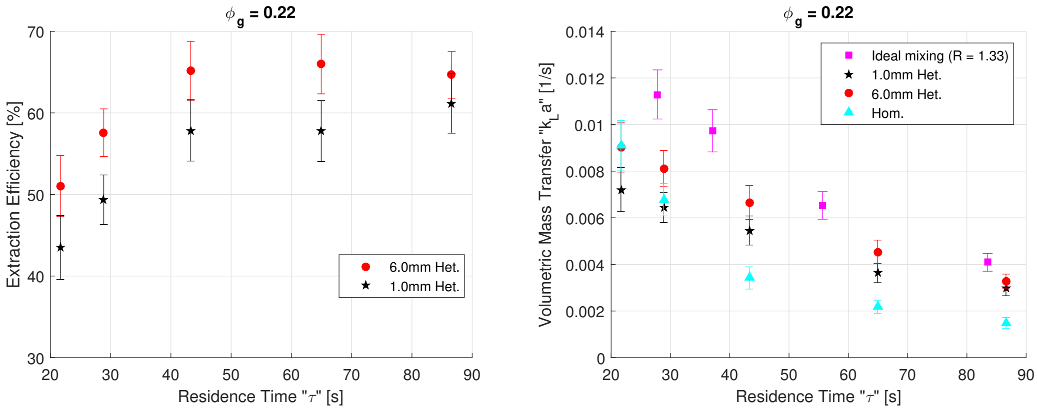

(a) (b)

Figure G.1: The extraction efficiency and volumetric mass transfer coefficient for the organic to water ratio of 1.33 and $\phi_g = 0.22$.

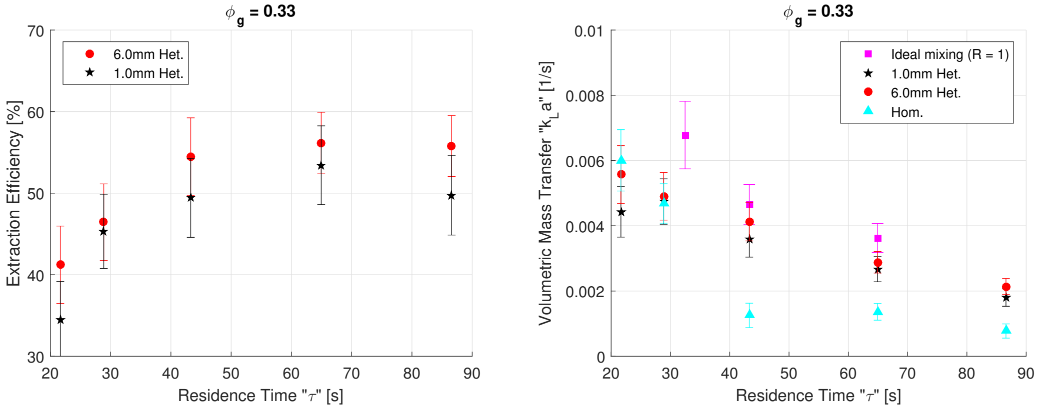

(a) (b)

Figure G.2: The extraction efficiency and volumetric mass transfer coefficient for the organic to water ratio of 1 and $\phi_g = 0.33$